DISSERTATIONES
SCIENTIAE
MATERIALIS
UNIVERSITATIS
TARTUENSIS
36

KRISTEL MÖLS

Metastable TiO_2-II in atomic layer deposited thin and ultrathin films: stabilization, properties and impact on film growth

DISSERTATIONES SCIENTIAE MATERIALIS UNIVERSITATIS TARTUENSIS

36

DISSERTATIONES SCIENTIAE MATERIALIS UNIVERSITATIS TARTUENSIS

36

KRISTEL MÖLS

Metastable TiO_2-II in atomic layer deposited thin and ultrathin films: stabilization, properties and impact on film growth

UNIVERSITY OF TARTU
Press

The study was carried out at the Institute of Physics, University of Tartu, Estonia.

The Dissertation was admitted on June 21, 2024, in partial fulfilment of the requirements for the degree of Doctor of Philosophy in Material Science and allowed for defence by the Scientific Council on Material Science of the Faculty of Science and Technology, University of Tartu.

Supervisors: Prof. Jaan Aarik, Institute of Physics, University of Tartu

Dr. Hugo Mändar, Institute of Physics, University of Tartu

Opponents: Dr. Sandra Stanionytė, Center for Physical Sciences and Technology, Vilnius, Lithuania

Dr. Tomáš Roch, Dr. techn., Faculty of Mathematics, Physics and Informatics, Comenius University Bratislava, Slovakia

Defense: August 28, 2024, University of Tartu, Estonia

This work has been partially supported by the Estonian Research Council (Grants PSG448 and PRG753),the Estonian Ministry of Education and Research (Grant IUT2-24), Estonian Science Foundation (Grant ETF-9088), Estonian-French science and technology cooperation program PARROT (Project “Optimization of Atomic layer Deposition methods for growing metal oxide thin films”), and EU through the European Regional Development Fund (Projects 3.2.1101.12-006, TK117, TK134, and TK141) and Graduate School of Functional materials and technologies.

European Union
European Regional
Development Fund

Investing
in your future

ISSN 2228-0928 (print)
ISBN 978-9916-27-596-2 (print)
ISSN 2806-2574 (pdf)
ISBN 978-9916-27-597-9 (pdf)

University of Tartu Press
www.tyk.ee

TABLE OF CONTENTS

LIST OF ORIGINAL PUBLICATIONS AND AUTHOR'S CONTRIBUTIONS

This thesis is based on the following original publications:

I. A. Tarre, **K. Möldre**, A. Niilisk, H. Mändar, J. Aarik, A. Rosental, "Atomic layer deposition of epitaxial TiO_2 II on c-sapphire", *Journal of Vacuum Science & Technology A: Vacuum Surfaces and Films*, 31 (1) (2013) 01A118-1–5, http://doi.org/10.1116/1.4764892.
The author of the thesis contributed to the paper by participating in the deposition of films. She was involved in most of the Raman spectroscopy measurements. She measured and analyzed X-ray diffraction patterns.

II. **K. Möldre**, L. Aarik, H. Mändar, A. Niilisk, R. Rammula, A. Tarre, J. Aarik, "Atomic layer deposition of rutile and TiO_2-II from $TiCl_4$ and O_3 on sapphire: Influence of substrate orientation on thin film structure", *Journal of Crystal Growth* 428 (2015) 86–92, https://doi.org/10.1016/j.jcrysgro.2015.07.029.
The author of the thesis determined the thickness, density, and surface roughness of the films using X-ray reflectivity, and characterized the structure of the films using X-ray diffraction methods. She also participated in some Raman spectroscopy studies, analysis of results, and writing the paper.

III. **K. Möls**, L. Aarik, H. Mändar, A. Kasikov, A. Niilisk, R. Rammula, J. Aarik, "Influence of phase composition on optical properties of TiO_2: Dependence of refractive index and band gap on formation of TiO_2-II phase in thin films", *Optical Materials* 96 (2019) 109335, https://doi.org/10.1016/j.optmat.2019.109335.
The author of the thesis conducted X-ray reflectivity studies to determine thickness, surface roughness, and density, characterized the structure of films using X-ray diffraction methods, carried out spectrophotometric measurements, performed analysis of results, and participated in writing the paper.

IV. **K. Möls**, L. Aarik, H. Mändar, A. Kasikov, T. Jõgiaas, A. Tarre, J. Aarik, "Influence of α-Al_2O_3 template and process parameters on atomic layer deposition and properties of thin films containing high-density TiO_2 phases", *Coatings* 11 (11) (2021) 1280, https://doi.org/10.3390/coatings11111280.
The author of the thesis carried out X-ray reflectivity studies to determine thickness, surface roughness, and density, determined the structure of the films using various X-ray diffraction methods, participated in spectrophotometric measurements, and performed analysis of the obtained data. She was involved in the hardness determination and participated in writing the paper.

LIST OF ABBREVIATIONS AND SYMBOLS

II	TiO_2-II
A	anatase
ALD	atomic layer deposition
c-sapphire	single crystal α-Al_2O_3 substrate, surface parallel to the (0 0 1) atomic plane
CVD	chemical vapor deposition
FWHM	full width at half maximum
GPC	growth per cycle
HRXRD	high resolution X-ray diffraction
MBE	molecular beam epitaxy
MOCVD	metalorganic chemical vapor deposition
PVD	physical vapor deposition
R	rutile
RHEED	reflection high energy electron diffraction
r-sapphire	single crystal α-Al_2O_3 substrate, surface parallel to the (0 1 2) atomic plane
S	substrate
SE	spectroscopic ellipsometry
SPM	spectrophotometry
XRD	X-ray diffraction
XRR	X-ray reflection
2θ	angle between the incident and diffracted X-ray beams
a, b, c	lattice parameters of crystalline phases
E_g	bandgap energy
$h\nu$	photon energy
n	refractive index
R	optical reflectance
t	film thickness
T	optical transmittance
T_G	growth temperature
α	absorption coefficient
φ	azimuthal angle characterizing the in-plane rotation of sample in XRD studies
ω	the angle of rotation of the sample around an axis perpendicular to the diffraction plane in XRD studies

1. INTRODUCTION

Titanium dioxide (TiO_2) is a material of great interest due to its unique properties. TiO_2 is used in the paint, paper, pharmaceutical, and cosmetics industries as a pigment and filler [1]. However, TiO_2 also attracts great interest in micro- and nanoelectronics because of its relatively high dielectric constant [2]. In optical coatings, the high refractive index and transparency of titanium dioxide in the visible spectral range are important. Photocatalytic films of TiO_2 are applied as self-cleaning and antibacterial coatings of surfaces [3]. Additionally, TiO_2 films are used in catalysts, gas sensors, and anti-corrosion coatings [4]. Depending on the applications of titanium dioxide, the requirements for its properties can be very different. In some cases, porous TiO_2 with a large specific surface area is needed, while in other cases, uniform thickness (*t*), high density, and/or surface smoothness of the material are important parameters of TiO_2 films [4].

Thin films of TiO_2 have been synthesized using both physical and chemical methods. Films produced by physical methods are typically purer, but it is difficult to achieve uniform thickness on complex-shaped surfaces with these methods. Films prepared by Chemical Vapor Deposition (CVD) may contain residues of starting materials but cover surfaces much more evenly. One of the best methods for depositing films with precisely controlled thickness is Atomic Layer Deposition (ALD). Films synthesized in this way cover complex-shaped surfaces very well [5]. Additionally, the thickness of the growing material layer is easy to control, as growth occurs in sequential cycles, one atomic layer or fractions thereof at a time.

Several physical and chemical properties of solid films depend on the phase composition and crystalline quality of materials. The structure, in turn, depending on the synthesis conditions and properties of substrate can also affect the growth rate of the films [6]. Naturally, for any application, it is important to know the properties of the produced material. Therefore, structural studies are very important in characterizing films, also allowing for a better understanding of the impact of growth process parameters on the film properties.

The effect of structure on the growth rate of TiO_2 in ALD processes has been quite thoroughly studied for films containing anatase and amorphous phases [6]. However, when the studies described in this thesis were initiated, much less information was known about ALD of rutile and, especially, the metastable TiO_2-II phase. Moreover, there was no sufficient information on the optical and mechanical properties, for instance refractive index, optical bandgap energy, and hardness of TiO_2-II.

The aim of this work was to investigate the structure, phase composition, growth rate, density, hardness and surface roughness of TiO_2 films synthesized by ALD, and dependence of these thin-film parameters on the substrate, deposition temperature, and film thickness, to primarily understand the peculiarities of the TiO_2-II phase growth and the properties of films containing this phase.

2. BACKGROUND

2.1 Polymorphs and properties of TiO_2

Anatase, rutile, and brookite are the most common TiO_2 phases, which all are stable at ambient conditions. In addition to these crystallographic phases, TiO_2 has a number of other polymorphs. Most of the latter polymorphs are called high-pressure phases, because they can be formed due to phase transitions occurring at high pressures [7]. When the pressure is increased, the phase transitions occur at normal temperatures in the order: rutile/anatase → TiO_2-II → M I → O I → O II [7]. It is believed that some high-pressure phases of TiO_2, for example phase O II, have the main properties similar to those of diamond [8]. However, there are also researches who claim that the mechanical properties of all high-density phases of titanium dioxide are similar [9].

One of the high-pressure phases, TiO_2-II, is stable even under normal conditions [10,11]. It is believed that rutile and TiO_2-II are energetically very similar, and TiO_2-II is even more stable than rutile at low compression [9]. The densities and elastic moduli of these phases are also similar (Table 1).

According to theoretical calculations [29], TiO_2-II with an orthorhombic lattice should have a much wider bandgap than rutile with a tetragonal lattice. In these calculations, bandgap energies (E_g) of 2.33 and 1.86 eV have been obtained for TiO_2-II and rutile, respectively [29]. However, it should be kept in mind that the E_g values obtained in such calculations often differ significantly from those measured in the experiment. For example, bandgap widths obtained from rutile measurements have ranged from 3.03 eV [30] to 3.16 eV [6]. At the same time, the bandgap width of anatase that has a lower density than rutile has been measured to be 3.3 eV [31]. Moreover, when the studies described in this thesis were started, there were no data on the refractive indices (n) of TiO_2-II in the literature, while the corresponding values of rutile and anatase were available in many publications (Table 2).

Table 1. Lattice constants, densities and elastic moduli of rutile and TiO_2-II.

Phase	a (Å)	b (Å)	c (Å)	Density (g/cm^3)	Elastic modulus (GPa)	Reference
Rutile	–	–	–	–	200–203	[9]
	4.952	4.952	2.961	–	–	[10]
	4.592	4.592	2.964	4.2485	230	[12]
	4.594	4.594	2.959	–	–	[13]
	4.56	4.56	2.96	–	–	[14]
	4.59	4.59	3.00	–	–	[15]
	4.593	4.593	2.935	–	241	[16]
	–	–	–	–	243	[17]
	–	–	–	–	210	[18]
	–	–	–	–	239	[19]
	–	–	–	–	229	[20]
	4.5938	4.5938	2.9586	–	195.3–200.4	[17]
TiO_2-II	–	–	–	–	206–208	[9]
	4.535	5.499	4.900	4.34	–	[10]
	4.535	5.495	4.901	–	–	[11]
	4.541	5.493	4.906	4.336	260	[12]
	4.59	5.44	4.94	–	–	[13]
	4.61	5.40	4.97	–	–	[14]
	4.58	5.42	4.96	–	–	[15]
	4.536	5.486	4.883	–	241	[16]
	–	–	–	–	250	[17]
	–	–	–	–	258	[18]
	–	–	–	–	264	[19]
	–	–	–	–	224	[20]
	4.541	5.492	4.906	–	193.9–206.8	[21]
	4.563	5.469	4.911	4.330	–	[22]
	4.515	5.497	4.939	4.329	–	[22]
	4.541	5.493	4.906	4.336	–	[23]
	4.61	5.43	4.87	–	–	[24]
	4.5337	5.4996	4.9037	4.341	–	[25]
	4.55	5.46	4.92	4.34	–	[26]
	4.487*	5.374*	4.804*	4.581*	–	[27]
	4.52	5.51	4.97	–	–	[28]

*measured at 10 GPa

Table 2. Refractive indices of TiO_2 films.

Phase composition*	Method of synthesis	Refractive index	Wavelength (nm)	Reference
(A+R), R	ALD	2.47–2.82	580	[6]
Am+A	ALD	2.3–2.5	580	[32]
A, R	ALD	2.65–2.7; 2.75	580	[33]
A	ALD	2.5	580	[34]
Am, A+R+Am	Magnetron sputtering	2.24–2.46	500	[35]
–	Electron beam evaporation	2.2–2.34	640	[36]
A, A+R	Sol-gel	1.95–2.5	500	[37]
A	Plasma deposition	2.20–2.45	550	[38]
A	Sol-gel	2.00–2.35	550	[39]
A	Electron beam evaporation	2.29	550	[40]
A	Sol-gel	2.26–2.44	550	[41]
A; R	Arc deposition	2.62; 2.72	550	[42]
A, A+B, R	Sol-gel	1.94 – 2.44	632.8	[43]
A, A-R	CVD	2.25–2.48	632.8	[44]
A, R	Laser ablation	2.21; 2.45	525	[45]
R	Electron beam evaporation	2.20–2.45	640	[46]
A, R	CVD	2.0–2.7	500–900	[47]
Am, A	Sol-gel	1.9–2.54	632.8	[48]

* A – anatase, Am – amorphous, B – brookite, R – rutile

2.2 Applications of TiO_2

TiO_2 is a dielectric that has high refractive index and is transparent in visible and near-infrared ranges of spectrum. These characteristics have rendered TiO_2 a material of significant interest for the development of high-refractive-index layers in optical waveguides [49–55] and for the fabrication of multilayer optical coatings [56–59]. Additionally, the optical non-linearity of TiO_2 [54,55,60] has facilitated its application in the wavelength conversion of signals within integrated optical devices [54,55] and sensors [60]. Beyond these applications, TiO_2 is widely researched and utilized as a potent photocatalyst [29,61–64]. The optical properties of bulk materials and thin films encompassing the amorphous, anatase, and rutile phases of TiO_2 have been extensively studied [31,42,65–73]. The influence of deposition process parameters on the optical constants of thin films containing these phases has been precisely documented [42,67,72,73]. Typically, films with a greater density are found to exhibit higher refractive index values [66,68,69]. Specifically, the density and refractive index of the rutile phase are noted to be superior to those of the amorphous and anatase phases of TiO_2

[42,71,72], underscoring the material's versatility and effectiveness across a range of applications.

Materials incorporating TiO_2-II are expected to be beneficial in several key technologies, including the production of hydrogen [74–76], development of lithium-ion batteries [77], and engineering of supercapacitors that exhibit a high energy density [78]. These applications frequently employ nanocrystalline powders [74–77] and nanowires [78]. The exceptional catalytic efficiency observed in the materials containing TiO_2-II also renders them promising candidates for functional coatings. Further, both the theoretical analyses [17] and experiments conducted under high pressures [12,23] have demonstrated that TiO_2-II possesses a bulk modulus superior to those of rutile and anatase, suggesting that the inclusion of TiO_2-II could enhance the hardness of functional coatings beyond what is achievable with the anatase phase that is traditionally known as catalytically effective form of TiO_2. It is important to note that significant additional data has emerged since the commencement of the work reported in this thesis.

2.3. Synthesis of TiO_2

2.3.1. General principles

For the industrial use, titanium dioxide is obtained from natural minerals. Chlorination of these minerals produces titanium tetrachloride ($TiCl_4$), which is then purified. Pure TiO_2 is obtained as a result of the reaction between $TiCl_4$ and O_2. During this process, TiO_2 is usually formed as anatase. If rutile form of TiO_2 is desired, aluminum chloride is added to titanium chloride.

There are several chemical and physical methods for producing TiO_2 films. Physical methods used for depositing TiO_2 films include electron beam evaporation and magnetron sputtering. The major chemical methods include CVD, sol-gel deposition, and ALD. A major advantage of ALD is the ability to coat very complex surfaces with precisely controlled thickness and to reproducibly grow very thin solid films.

TiO_2-II does not occur naturally in the pure form. This phase has been found associated with rutile [10,14,15,79]. TiO_2-II has also been obtained by hydrothermal growth [11,25] and by grinding anatase-phase TiO_2 [12,18]. Thin films containing TiO_2-II have been obtained by CVD [80] pulsed laser deposition [24] and ALD [27,28].

2.3.2 Atomic layer deposition

Atomic layer deposition is a cutting-edge thin-film synthesis technique with a rapidly expanding role in various fields of science and technology. For example, ALD films are used in semiconductor devices as gate dielectrics, interconnects, and high-k dielectrics of capacitors [81]. ALD has also been employed for fabrication of fuel cell and supercapacitor components [82,83]. In optoelectronics, ALD films are used in antireflection coatings, photonic structures, and optoelectronic devices [52,54,67]. In addition, ALD can be applied in synthesis of catalysts for various chemical processes [84].

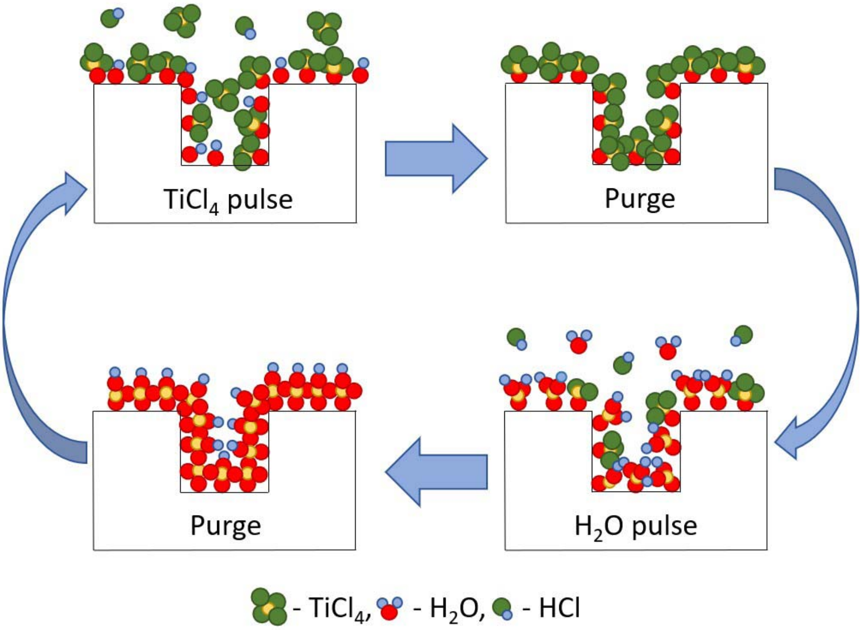

Figure 1. Schematic representation of an ALD process using $TiCl_4$ and H_2O as precursors. The representation is based on the results of real-time quartz crystal microbalance studies [5].

ALD is a cyclic process that deposits thin films with atomic-layer or even subatomic-layer resolution. It is based on self-limiting surface reactions, ensuring a uniform and highly controlled film growth. The cyclic nature of ALD also reduces the concentration of defects in films because the surface reactions are self-terminated. This contributes to the enhanced quality and reliability of films grown by ALD.

The simplest ALD processes typically involve 4 steps (*Fig. 1.*).

- The surface of a substrate or growing film is exposed to the vapor of the first precursor ($TiCl_4$ in Fig. 1) that chemisorbs onto the surface, forming a monolayer of intermediate surface species.
- Excess precursor and gaseous reaction by-products are purged from the reaction chamber to avoid gas-phased reactions during the next reaction step.
- The solid surface is exposed to the vapor of the second precursor (H_2O in Fig. 1), which reacts with the intermediate surface species to form a solid compound.
- The remaining precursor and gaseous by-products are purged from the reaction chamber.

The cycle is repeated until the desired film thickness is achieved.

ALD can deposit a broad range of materials, including oxides, nitrides, metals, and organic materials. This versatility enables the development of diverse device structures and functionalities. However, the selection of appropriate precursors is crucial for the success of any ALD process [85]. The precursors should be volatile enough to be easily vaporized and transported to the reactor, sufficiently reactive to chemisorb onto the surface of a substrate or growing film during the exposure stage, stable during storage and handling to prevent decomposition, polymerization, or hazardous reactions. Precursors should have well-defined vaporization and decomposition temperatures that are compatible with the desired growth conditions. The reactions of precursors with the substrate material should be self-limiting to avoid the damage of the substrate during the ALD process [85].

The choice of precursors also impacts the chemical composition, structure, and properties of films deposited. Therefore, the desired film characteristics should always be considered during the precursor selection.

The growth temperature (T_G), that is the substrate temperature, used for deposition of a film, plays an essential role in determining the growth mechanism in ALD. As a result, the variation of T_G allows for the adjustment of growth rate and material properties obtained. Each ALD reaction has an associated activation energy, which determines the reaction rate. By varying the temperature, one can control the activation energy and, consequently, the reaction rate. A higher temperature generally leads to faster reactions. However, as the ALD processes are based on self-limited reactions, when precursor pulses with sufficient durations are used and no changes in the reaction mechanisms occur, the increase in the reaction rate does not have to cause any increase in the growth per cycle (GPC). However, at T_G that is too high, the precursors may decompose or some reaction products that should form the solid film may desorb. As a result, marked dependence of GPC on T_G can appear in this temperature range. With decreasing temperature, the reaction rate decreases and at too low T_G, the precursors may condense on the surface or not react with the surface at all. Therefore, considerable dependence of GPC on T_G can also appear at too low temperatures. At intermediate temperatures, the effect of T_G on GPC is relatively weak.

The substrate temperature also affects the crystallinity of the deposited film. A higher T_G can promote the growth of crystalline films, while lower T_G tends to yield amorphous or mixed-phase films. This effect allows for tailoring the material properties to suit specific applications [85].

Atomic layer deposition is appealing because the self-limited nature of surface reactions allows for easy control over the film thickness, ensures the repeatability of the deposition process, and enables covering surfaces of very complex shapes with a film with uniform thickness. One of the most significant advantages of ALD is its ability to control the film thickness at the atomic-layer level. This makes the method ideal for applications where tight control over the film thickness is essential, particularly in semiconductor industry, nanotechnology, and technology of advanced functional coatings. In these applications, ALD provides exceptional conformality, which is vital for coating complex structures like nanoparticles, high-aspect-ratio substrates, and nanotemplates.

On the other hand, ALD is a time-consuming process, with deposition rates significantly lower than those in some other techniques like CVD or sputtering. It can take several hours to grow a film with a thickness of a few hundred nanometers by ALD. In the cases where the surface reactions are not fully completed, a film deposited by ALD may contain residual impurities, which affect the properties of the film [85]. Therefore, the growth rate and properties (for instance, structure, density, and roughness) of the synthesized films depend on both the starting materials and the growth temperature [28,67,72,73,86–93].

Depending on the growth conditions and substrate, the films can be grown either epitaxially or non-epitaxially. Epitaxy refers to the ordered growth of one crystalline material to the surface of the other crystalline material. Non-epitaxial films do not have a crystallographic relationship with the substrate. These films are typically amorphous or polycrystalline. While they may lack the strict structural control of epitaxial films, non-epitaxial films are still valuable in many applications, such as anti-reflective coatings, passivation layers, and insulating materials. Epitaxial ALD films exhibit a crystallographic relationship with the underlying substrate. This relationship ensures the growth of a crystalline film with a well-defined orientation and lattice matching to the substrate. Epitaxial growth, thanks to the highly ordered crystal structure obtained, ensures high density and homogeneity of the film material. Additionally, the crystallographic relationship between the substrate and growing film can also affect the growth rate of the film. Epitaxial ALD is often sought in semiconductor manufacturing and other applications where strict crystallographic control and interfaces with low defect concentrations are needed.

The epitaxial growth in ALD as well as in other thin-film deposition processes is influenced by several factors. The quality and orientation of the substrate surface play a major role in epitaxial growth. A well-prepared, single-crystal substrate surface is more likely to promote epitaxial films. To grow an epitaxial film, the crystal lattices of the film and the substrate must match well enough. At the same time, the matching of lattices can be sufficient for epitaxy even in the cases where the lattice types of the substrate and the film, and some of the lattice parameters are different. It is important that the two-dimensional unit cells of the crystal lattices of the substrate and film match with each other [94]. One such example of epitaxial growth is the growth of tetragonal TiO_2 with the rutile structure (cell parameters in Table 1) on α-Al_2O_3 with the trigonal structure and lattice constants depicted in Table 3.

Choosing the precursors that can chemisorb and react specifically with the substrate surface is essential for epitaxial growth. The substrate temperature and precursor pressure also affect the epitaxial growth in an ALD process. Optimizing these parameters enhances epitaxial film quality. For instance, atomic layer epitaxy requires relatively high T_G and, thus, necessitates the use of precursor combinations that perform well at higher T_G. However, compared to CVD, ALD can facilitate the epitaxial growth of materials like TiO_2 at somewhat lower temperatures.

Table 3. Lattice constants of α-Al_2O_3.

	a (Å)	c (Å)	Reference
α-Al_2O_3	4.7493	12.9647	[95]
	4.7582*	12.9883*	[96]
	4.763	13.006	[97]
	4.759	12.991	[98]
	4.758	12.991	[99]

*determined at 250 K.

In ALD of TiO_2, several precursor pairs and substrates have been used. The earliest works employed $TiCl_4$ and H_2O as the precursors. This precursor system has been extensively studied, particularly in the T_G range of 100–600 °C [28,67, 72,86–88,90]. Material deposited from the $TiCl_4$-H_2O process at lower substrate temperatures contains chlorine residues, which hinder crystallization processes. Thus, films obtained at lower temperatures are amorphous and more susceptible to etching [86,87,90]. In the T_G range of 165–350 °C, the anatase phase of TiO_2 has predominantly formed in non-epitaxial films. At higher temperatures, rutile begins to form [67,87]. It has also been established that increasing the growth temperature decreases the growth per cycle [67, 86], unless any detectable changes in the phase composition of the film material appear. In the T_G range where the growth of the amorphous phase is replaced by the anatase growth, the temperature rise leads to an increase in growth rate [88]. Epitaxial TiO_2 films were grown on α-Al_2O_3(0 1 $\bar{1}$ 2) (r-sapphire) and α-Al_2O_3(0 0 0 1) (c-sapphire) substrates in the $TiCl_4$-H_2O process at T_G exceeding 400 °C [72].

Organic compounds, such as titanium(IV) ethoxide ($Ti(OCH_2CH_3)_4$) [34,100], titanium(IV) isopropoxide ($Ti(OCH(CH_3)_2)_4$) [32,89,101], and titanium(IV) methoxide ($Ti(OCH_3)_4$) [84] have been quite commonly used as titanium precursors. The $Ti(OCH_2CH_3)_4$ process is well applicable in the temperature range of 100–250 °C [34]. Above 250 °C, $Ti(OCH_2CH_3)_4$ begins to decompose, but films with relatively uniform thickness can still be grown at temperatures up to 350 °C. The films grown at temperatures of 180–350 °C have contained polycrystalline anatase while those deposited at lower temperatures have been amorphous [34]. When T_G increased, the refractive indices of films increased [34]. The growth rate also increased with the deposition temperature [34,100].

$Ti(OCH(CH_3)_2)_4$ begins to decompose at temperatures above 300 °C [32,89]. Compared to the $TiCl_4$-H_2O process, the deposition rate in the $Ti(OCH(CH_3)_2)_4$-H_2O process is lower [32,89]. However, the deposition rate can be increased by using H_2O_2 instead of H_2O as the oxygen source [89]. With an increase in T_G, the refractive index of the film material also increases [32]. The deposited films typically contain amorphous and anatase phases [32,89,101].

If titanium(IV) methoxide ($Ti(OCH_3)_4$) is used as the precursor, the deposition temperature can be increased up to 400 °C [102]. At $T_G \geq 250$ °C, the films deposit as polycrystalline anatase, while at lower temperatures, the film remains amorphous.

The highest T_G of titanium dioxide films deposited using TiI_4 and H_2O_2 [33,103], TiI_4 and H_2O [104], and TiI_4 and O_2 [91] as the precursors has been at 490 °C. When a mixture of H_2O and H_2O_2 was used as the oxygen source, the refractive index [33] and growth rate [33,104] increased with T_G. On polycrystalline Si substrates, the anatase phase of TiO_2 was formed [33], while on r- and c-sapphire substrates epitaxial rutile and on MgO(0 0 1) substrates epitaxial anatase grew. The epitaxial growth was observed at $T_G \geq 230$ °C on MgO(0 0 1), $T_G \geq 230$ °C on r-sapphire, and $T_G \geq 375$ °C on c-sapphire [103]. Using TiI_4 and pure oxygen, epitaxial films were also successfully grown on α-Al_2O_3(0 1 $\bar{1}$ 2) and MgO(0 0 1) substrates, with rutile growing epitaxially on α-Al_2O_3(0 1 $\bar{1}$ 2) substrates at 455 °C and anatase growing epitaxially on MgO substrates at 375 °C [91].

In the ALD processes, where H_2O is one of the precursors, reactions generally occur via hydroxyl groups. However, films obtained from such reactions often contain hydrogen, which is not permissible for many applications requiring high-purity films. Therefore, hydrogen-free precursors have been studied for depositing oxides [73,91]. As mentioned earlier, TiI_4 and O_2 have enabled the synthesis of TiO_2 films via the ALD method. The resulting films contained less than 0.1% iodine residues. It was also determined that at $T_G > 200$ °C, the absence of hydroxyl groups on the surface did not affect the growth rate and that it was possible to synthesize both anatase and rutile epitaxially [91]. However, major drawbacks of using TiI_4 as an at ALD precursor is related to its relatively low vapour pressure and highly corrosive effect on materials used in the construction of ALD reactors.

In the ALD process using $TiCl_4$ and O_3 as the precursors, it was possible to grow anatase and, at higher temperatures, also rutile on Si(1 0 0) substrates. In the T_G of 350–500 °C, the growth rate was even higher than that in the process where H_2O was used as the oxygen source. Additionally, the films deposited at temperatures of 350–400 °C were relatively smooth [73]. Based on these results, the current work has been planned with the aim to elucidate the peculiarities of TiO_2 epitaxial growth from these precursors.

2.4 Earlier studies of TiO_2-II

Over the past several years, there has been a notable surge in the exploration of the TiO_2-II phase for various applications [62,74–78,105–108]. The TiO_2-II phase has been synthesized from other TiO_2 crystalline forms through methods such as high-pressure compression [12,22,23,26,74,77,109–113], ball milling [62,106,114,115], and high-pressure torsion [75,76,105,116]. TiO_2-II has also been produced in single crystals via high-pressure hydrothermal methods [7,11,25,117], in powders by flame techniques [118,119], and in thin films using various deposition methods including metalorganic chemical vapor deposition (MOCVD) [80], ALD [118,119], vapor-liquid-solid [107], and spray pyrolysis [108].

Often, TiO_2-II appears as an intermediate phase in the transformation from anatase to rutile, facilitated by ball milling [62,106,114,115], and in thin films during similar transition conditions [119]. Its presence alongside anatase and/or rutile in various materials [25,75,76,106,115,116,118,119] makes the combined application of these phases more appealing and practical than using pure TiO_2-II alone. The superior catalytic properties of such phase combinations have been theoretically predicted [63,64] and experimentally verified [75,76]. Furthermore, the complex optical properties of these mixtures defy simple predictions based on the pure phases, suggesting a need for more comprehensive research on TiO_2-II mixtures [63,64].

It is noteworthy in this connection, that often optical properties of materials can more conveniently be determined in studies of thin films. The focus on thin films, rather than powders or single crystals, is also driven by the demands of numerous applications. Earlier TiO_2-II has been obtained in thin films through methods like MOCVD [80], ALD [118,119], vapor-liquid-solid [107], and spray pyrolysis [108], with ALD enabling precise thickness control and the ability to coat intricately shaped surfaces.

Previously, the growth of TiO_2-II phase in ALD processes has been revealed by the reflection high energy electron diffraction (RHEED) method in non-epitaxial films grown by ALD on Si substrates within a suitable range of growth temperatures (375–550 °C), precursor doses, and film thicknesses [28]. It was believed that TiO_2-II formed due to oxygen vacancies and/or internal stresses in the films [28,120]. Additionally, TiO_2-II has been observed by the transmission electron microscopy (TEM) in the films grown by ALD from $TiCl_4$ and H_2O on KBr [118]. However, the results of more recent investigation indicated that the electron beam excitation used in RHEED and TEM studies probably contributed to the formation of TiO_2-II, as no considerable amounts of TiO_2-II were observed by Raman spectroscopy and X-ray diffraction in the films that contained this phase according to RHEED data [119].

3. RESEARCH OBJECTIVES

The aim of this work was to investigate how substrate materials, precursors, and deposition process parameters influence the phase composition of atomic-layer-deposited titanium dioxide thin films. In particular, the work was focused on identification of optimal process parameters, including temperature and ALD cycle time parameters, permitting to achieve the highest concentration of the high-pressure TiO_2-II phase in the films.

It was expected that the epitaxial growth of TiO_2 on sapphire substrates could support formation of crystalline TiO_2 phases in the films. Therefore, the investigation of the phase composition in the films grown on sapphire substrates with different orientations was one of the main tasks of the research. An important objective of the study was to analyze the epitaxial relationships for coexisting TiO_2-II and other crystalline phases in the films. A related objective was to examine how the growth rate of the films depended on the crystal phases formed.

Furthermore, the research was expected to lead to understanding how to manipulate the deposition process parameters to attain the desired phase composition and properties of the titanium dioxide thin films. A comparison between the $TiCl_4$-H_2O and $TiCl_4$-O_3 ALD processes was performed to understand the impact of the oxygen precursor on the phase composition and properties of the titanium dioxide thin films grown by ALD. The research was also targeted to delve into how the precursor dosing affects the relative amount of TiO_2-II in the films. Determining the possible influence of the film thickness on the relative amount of different crystal phases in the films was also a goal of marked interest in the studies carried out.

With the aim to understand, how the formation of TiO_2-II influenced other properties of TiO_2 films, the refractive index, bandgap energy, and hardness of the films containing TiO_2-II phase were determined and compared with corresponding parameters of anatase and rutile films. Such insights are crucial for applications spanning from semiconductor devices to photocatalysis, offering avenues for further exploration and innovation in the field of thin film materials science.

4. EXPERIMENTAL METHODS

4.1 Growth of TiO_2 films

The TiO_2 thin films investigated in this work were deposited in low-pressure flow-type ALD reactors. In one reactor [121], the films were deposited using $TiCl_4$ and H_2O as the precursors [**I**] while in another reactor [122], the films were grown from $TiCl_4$ and O_3 [**II–IV**]. In both reactors, nitrogen (N_2, 99.999%) was used as the carrier gas. The carrier gas flows in the reactors were 140 and 230 sccm, respectively. However, since the reaction chamber cross-section area of the former reactor was smaller than that of the latter one, the linear gas velocities were around 3 m/s at a pressure of 220 Pa and T_G of 300 °C in both reactors. The precursor pulses were determined with computer-controlled solenoid valves. The temperature control was monitored with a thermocouple.

In all growth experiments, the films were deposited on c-sapphire and r-sapphire substrates. Prior to loading into the reactor, the substrates were cleaned in a hot solution of H_2SO_4 and H_2O_2 (5:2) for 5 minutes and rinsed in deionized water. This procedure was followed by a 30-second treatment with a 7% HF aqueous solution and another rinsing with deionized water. In some experiments, the films were deposited on fused silica (SiO_2) substrates too. The latter substrates were ultrasonically cleaned in ethanol and then rinsed in deionized water.

After loading the substrates into a reactor, the carrier gas flow was switched on, the reactor was pumped down to a pressure of 200–240 Pa, and the reaction zone was heated up. After stabilization of required T_G, the deposition process was started. In the first step of an ALD cycle, which was repeated to deposit a film, $TiCl_4$ vapor was led into the growth chamber. In the next step, the chamber was purged with the carrier gas. After that, either H_2O or O_3 vapors were led into the growth chamber and the chamber was again purged with the carrier gas. The durations of the precursor pulses were determined by the open periods of solenoid valves.

In the $TiCl_4$-H_2O processes [**I**], the T_G values were varied from 350 to 680 °C, and the number of growth cycles ranged from 1250 to 3000. Each cycle included $TiCl_4$ exposure for 0.5 or 2 s, purging for 2 s, exposure to H_2O for 2 s, and another purge for 2–5 s. In the $TiCl_4$-O_3 processes [**II–IV**], the T_G values were varied between 250 and 600 °C, the numbers of ALD cycles ranged from 150 to 2800, while the $TiCl_4$ pulse, purge, O_3 pulse, and the second purge durations were 2–5 s, 2–5 s, 1–5 s, and 5 s, respectively.

4.2 Characterization of films

The crystal structure was examined using Raman spectroscopy and X-ray diffraction (XRD) techniques. Raman spectra were acquired with an inVia spectrometer (Renishaw) using a 514 nm laser beam for excitation. Raman shifts were recorded in the range 100–700 cm^{-1}. XRD analyses were conducted on a Smartlab diffractometer (Rigaku) in medium resolution point focus, grazing incidence (GIXRD), and high-resolution (HRXRD) modes. The HRXRD mode utilized Ge(220) two bounce monochromator and analyzer for yielding Cu Kα1 radiation, whereas just slit collimators and both Kα1 and Kα2 radiations were employed in the other modes that included also either polycapillary optics (point focus) or parallel slit analyzer (GIXRD) for the medium resolution studies. Identification of crystalline phases was based on the diffraction data in International Centre of Diffraction Data (ICDD) PDF-2 2015 database and structure data in Inorganic Crystal Structure Database (ICSD, FIZ Karlsruhe). Film characteristics such as thickness, density, and surface roughness were derived from X-ray reflection (XRR) patterns, recorded with the same diffractometer. The obtained diffraction and reflection data were processed using the programs GlobalFit, PDXL (Rigaku) and AXES [123].

Refractive index values, were measured using a GES5E spectroscopic ellipsometer (Semilab) with SEA software (Semilab), setting incident angles at 70°, 78°, and 75° for the measurement of the films deposited on SiO_2, r-, and c-sapphire substrates, respectively. A two-layer model was employed to calculate the refractive index, extinction coefficient, and thickness from the ellipsometry data. Absorption coefficient (α) values were calculated from transmission and reflection spectra, measured with a V-570 spectrophotometer (Jasco Corp.) in the wavelength range of 250–750 nm. A spectral slit width of 2 nm was chosen for the measurements.

Hardness values were assessed using a Triboindenter TI980 (Bruker) with a Berkovich diamond tip. Calibration was performed in continuous stiffness measurement mode against a fused silica standard (Bruker) with known hardness and modulus values. The strain rate and tip vibration frequency were maintained at 0.05 nm/s and 220 Hz, respectively, throughout calibration and subsequent film measurements on both c- and r-sapphire substrates. The standard deviation for hardness and modulus from a single calibration was approximately 1.5 GPa and 0.2 GPa, respectively. Each sample underwent thirty separate continuous stiffness measurements, with a maximum drift of 0.05 nm/s considered acceptable for a measurement.

5. RESULTS AND DISCUSSIONS

5.1 Phase composition

5.1.1 Results of Raman spectroscopy studies

Figure 2 shows Raman spectra of films grown on c-sapphire from $TiCl_4$ and H_2O (Figure 2a,b) using $TiCl_4$ pulse, purge, H_2O pulse, and purge periods with durations of 0.5, 2, 2, and 5 s, respectively, and from $TiCl_4$ and O_3 (Figure 2c) using $TiCl_4$ pulse, purge, O_3 pulse, and purge periods with durations of 2, 2, 5, and 5 s, respectively. The thicknesses of the films (*t*) were 11–17 nm (Figure 2a), 50–60 nm (Figure 2b), and 23–45 nm (Figure 2c). The anatase phase was detectable in the 12–18 nm thick films grown at $T_G \leq 425$ °C (Figure 2a) and 50–60 nm thick films grown at $T_G \leq 450$ °C (Figure 2b) from $TiCl_4$ and H_2O. The Raman spectra of the films deposited at $T_G \geq 425$ °C contained clearly distinguishable spectral lines at ~175, ~325, ~428, ~540, and ~605 cm^{-1} (Figure 2b). All these lines may belong to the TiO_2-II phase [10].

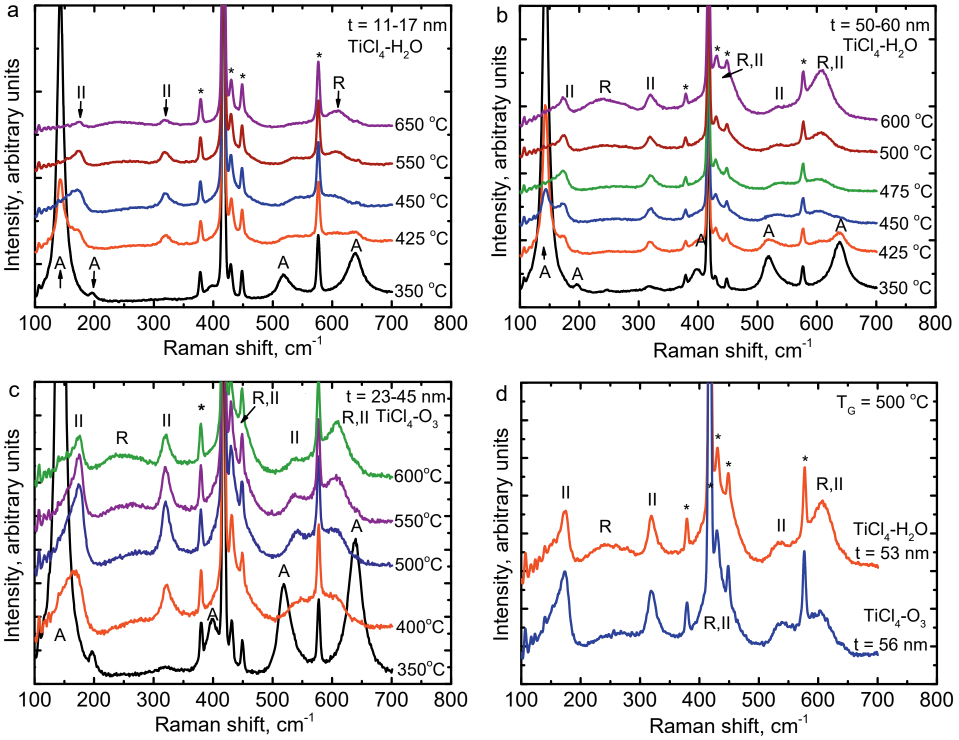

*Figure 2. Raman spectra of films grown on c-sapphire (a–c) at various temperatures using (a,b) $TiCl_4$-H_2O [**I**] and (c) $TiCl_4$-O_3 processes [**II**], and (d) at 500 °C in the $TiCl_4$-H_2O and $TiCl_4$-O_3 processes. Labels at spectral lines denote Raman bands attributable to anatase (A), rutile (R), TiO_2-II (II), and substrate (*).*

However, the lines observed at ~428, ~540, and ~605 cm^{-1} also coincide with the Raman scattering bands of rutile [10]. Therefore, the presence of TiO_2-II, can be assessed basing only on the Raman scattering bands peaking at ~175, ~325, and ~540 cm^{-1}.

Anatase was also detectable in the films, which were grown on c-sapphire from $TiCl_4$ and O_3 at 250–350 °C [**II,IV**]. No Raman bands of rutile and TiO_2-II were detected in the spectra of films deposited at T_G = 250–300 °C (Figure 1a of Ref. **II**). However, it should be noted that the sensitivity of Raman scattering method for rutile and TiO_2-II is lower than that for anatase [**IV**]. Hence, based solely on Raman scattering measurements, it cannot be claimed that these films contained no rutile and TiO_2-II at all. Lines attributed to TiO_2-II appeared in the Raman spectra, when T_G was raised to 350 °C, and became dominant in the spectra of films grown at 400–550 °C (Figure 2c).

When T_G was increased from 475–500 °C to higher temperatures, the relative intensity of Raman bands attributed to the TiO_2-II phase decreased in the Raman spectra, while the intensity of the bands attributed to rutile increased (Figure 2a–c). This result suggests that at higher growth temperatures, the proportion of rutile in the films began to increase.

The results presented in Figure 2a,b indicate that the T_G range, where TiO_2-II was preferentially formed, became narrower with increasing film thickness. In addition, basing on Figure 2a–d, it can be concluded that the films deposited from $TiCl_4$ and O_3 contained a higher concentration of TiO_2-II than those grown from $TiCl_4$ and H_2O using similar ALD process parameters. As the content of TiO_2-II also depended on the ALD cycle time parameters, particularly on the $TiCl_4$ pulse duration [**I,IV**], Raman spectra of films with similar thicknesses, grown in the $TiCl_4$-H_2O and $TiCl_4$-O_3 processes at 500 °C using the $TiCl_4$ pulse duration of 2 s in both processes, are compared in Figure 2d. This comparison confirms that TiO_2-II was more preferentially formed from $TiCl_4$ and O_3 than from $TiCl_4$ and H_2O.

Although the relative amount of TiO_2-II decreased and that of rutile increased with the increasing thicknesses of films deposited from $TiCl_4$ and H_2O at 500 °C [**I**] and from $TiCl_4$ and O_3 at 450–500 °C [**IV**], the influence of thickness on phase composition was relatively weak in the thickness ranges of 6.5–146 nm [**I**] and 14–88 nm [**IV**] of these films.

Figure 3, illustrates the effect of film thickness on the Raman spectra of films grown from $TiCl_4$ and O_3 on c-sapphire at 450 °C. For deposition of the films represented in this figure, the number of ALD cycles were varied from 150–1600. As can be seen in Figure 3, the thickness that was varied from 14 to 69 nm had no considerable effect on the phase composition. These results are in line with those of earlier studies [**IV**]. However, in the Raman spectrum of the 2.9 nm film, a weak anatase peak, which was no longer present in the Raman spectra of thicker films, was distinguishable (Figure 3). This suggests that as long as the growth is island-like in the very beginning of the deposition process, the anatase phase forms, but when the film becomes continuous, internal strain increases, leading to the formation of TiO_2-II/rutile.

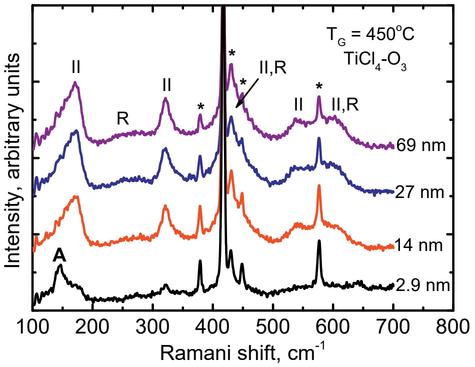

Figure 3. Raman spectra of films grown from $TiCl_4$ and O_3 on c-sapphire at 450 °C by applying different numbers of ALD cycles. The film thicknesses and origin of spectral lines of anatase (A), rutile (R), TiO_2-II (II), and substrate (*) are shown in the figure.

As mentioned already, the results obtained for films grown in the $TiCl_4$-H_2O process showed that the $TiCl_4$ dose also influenced the concentration of TiO_2-II in the films [**I**]. The relative amount of TiO_2-II phase increased and the contents of anatase and rutile decreased with increasing $TiCl_4$ exposure time [**I**]. The further studies of films grown at 350 °C in the $TiCl_4$-O_3 process revealed that the decrease in the O_3 pulse duration from 5 to 2 s and the following increase in the $TiCl_4$ pulse and the first purge durations from 2 to 5 s caused an increase in the relative amount of TiO_2-II in the films [**IV**]. A different relationship between the TiO_2-II content and the time parameters of the ALD process was observed for films deposited at 500 °C. Raman spectra of these films revealed that reducing the duration of O_3 pulse, increasing the duration of $TiCl_4$ pulse, and extending the subsequent purge time at 500 °C, which had favoured the growth of TiO_2-II at 350 °C, inhibited the growth of this phase compared to that of rutile [**IV**]. Thus, optimizing the time parameters of the process allowed for lowering the temperature for the most efficient growth of TiO_2-II, but did not widen the temperature range for the preferential growth of this phase significantly [**IV**].

Figure 4 demonstrates that unlike the films grown on c-sapphire, the films grown on r-sapphire and amorphous SiO_2 did not contain the high-pressure TiO_2-II phase [**II–IV**]. The Raman spectra of the films deposited on r-sapphire (Figure 4a) and SiO_2 (Figure 4b), revealed the formation of rutile and anatase, respectively [**II–IV**]. Traces of anatase were also detected in the films deposited on r-sapphire at 250 °C (Figure 4a).

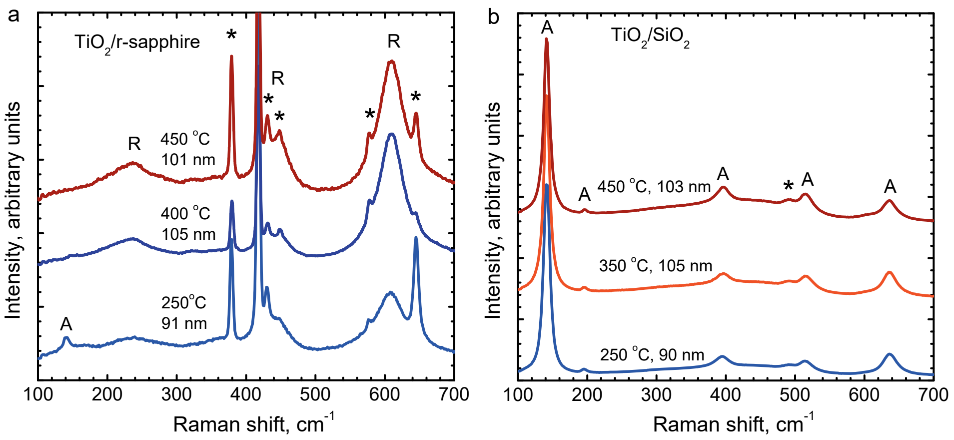

*Figure 4. Raman spectra of TiO_2 films grown on (a) r-sapphire and (b) SiO_2 substrates at various temperatures using the $TiCl_4$-O_3 process [**IV**]. Raman bands attributable to anatase (A), rutile (R), TiO_2-II (II) and substrate (*) are labelled correspondingly.*

5.1.2 Results of X-ray diffraction analysis

Figure 5 depicts HRXRD patterns of TiO_2 films deposited from $TiCl_4$ and H_2O (Figure 5a) and $TiCl_4$ and O_3 (Figure 5b) on c-sapphire. The vertical dash-dot-lines show the reference positions of the anatase 0 0 4, 1 1 2 and 2 2 4 reflections (ICDD PDF-2 card number 84-1286). The dashed lines indicate the reference positions of the rutile 2 0 0 and 4 0 0 reflections (ICDD PDF-2 database card 78-2485). The dotted lines mark the locations of the TiO_2-II 2 0 0 and 4 0 0 reflections, corresponding to the structure data of TiO_2-II in ICSD collection code 158778.

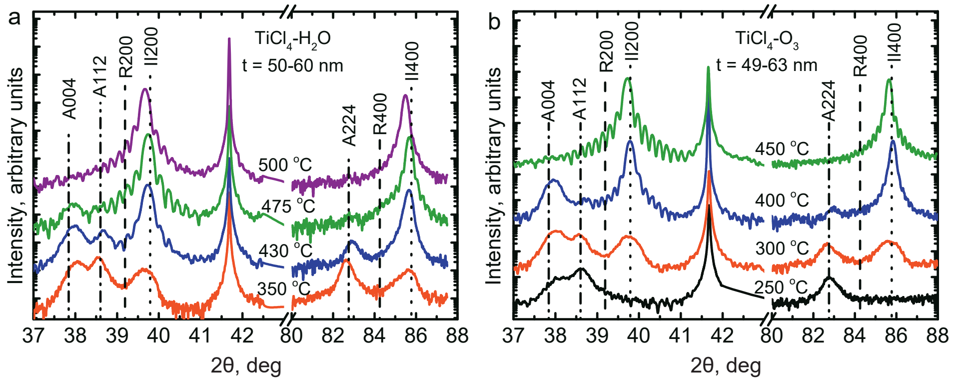

*Figure 5. Symmetrical θ–2θ scan diffraction patterns of films grown on c-sapphire at different temperatures using (a) the $TiCl_4$-H_2O process [**I**] and (b) the $TiCl_4$-O_3 process [**II**]. Vertical lines show reflection positions of anatase (A), rutile (R), and TiO_2-II (II). The reflection at 41.7° originates from the substrate.*

Looking at Figure 5a, one can see that at 350–475 °C, anatase as well as rutile and/or TiO_2-II were formed in the films deposited from $TiCl_4$ and H_2O. At higher T_G, films containing only rutile and/or TiO_2-II grew in this ALD process on c-sapphire as demonstrate the HRXRD data presented in Figure 5a and published earlier [**I**]. For comparison, in the HRXRD patterns of the films with similar thicknesses grown via the $TiCl_4$-O_3 process, the anatase and rutile/TiO_2-II reflections were of comparable intensity, when the films were deposited at 300–400 °C (Figure 5b). In the diffraction patterns of films grown at 250 °C, only the anatase reflections in addition to the reflections of c-sapphire were observed (Figure 2b) while in the films deposited at 450 °C (Figure 2b) and higher temperatures (Figure 2a of Ref. **II**), only rutile and/or TiO_2-II was detectable by HRXRD.

The diffractograms depicted in Figure 5 show that the T_G increase from 350 to 430 °C in the $TiCl_4$-H_2O process and from 250 to 300 °C in the $TiCl_4$-O_3 process altered the intensity ratios of the anatase 0 0 4 and 1 1 2 reflections (Figure 5). These changes in the anatase reflection intensities were in correlation with formation of rutile/TiO_2-II and corresponding appearance and increase in the intensities of the 2 0 0 and 4 0 0 reflections of rutile/TiO_2-II (Figure 5).

The 2 0 0 and 4 0 0 reflections of rutile/TiO_2-II were closer to the reference values of TiO_2-II (Figure 5) in the diffractograms of all films deposited on c-sapphire at temperatures up to 600 °C in our experiments [**I,II,IV**]. However, the increase in T_G caused these reflections to shift towards the reference positions of rutile reflections [**I,II**]. From this result, it can be inferred that raising the growth temperature increases the rutile content in the films. This result is consistent with the Raman spectroscopy data (Figure 2a). It was also observed that in the HRXRD patterns of films deposited at T_G of 400–500 °C, relatively strong Pendellösung fringes appeared at the rutile/TiO_2-II reflections, suggesting that a well-ordered epitaxial structure was formed in these films.

Pendellösung fringes were present in the diffraction patterns of the films deposited in both processes studied in the present work. However, in the diffraction patterns of the films grown from $TiCl_4$ and H_2O they were not as clearly visible as in those of the films grown from $TiCl_4$ and O_3. This indicates that films grown via the $TiCl_4$-O_3 process had better crystalline quality and lower mosaicity than the films deposited in $TiCl_4$-H_2O process. Therefore, the $TiCl_4$-O_3 process is more suitable for synthesizing high-quality rutile/TiO_2-II films than the $TiCl_4$-H_2O process. It can also be mentioned that basing on the relative intensities and positions of the rutile/TiO_2-II reflections, one can conclude that the T_G range of 450–500 °C was the most favourable one for the formation of the TiO_2-II phase [**I,II,IV**].

Results of rocking curve (ω-scan) measurements strongly supported the conclusion about high structural quality of films deposited on c-sapphire. In the case of films deposited on c-sapphire at 400–600 °C in the $TiCl_4$-O_3 process, the full width at half maximum (FWHM) values markedly lower than 0.1° were obtained for the 39.8° as well as for the 85.7° reflection. No significant dependence of the FWHM values on T_G was observed in this T_G range for the films deposited from $TiCl_4$ and O_3. For comparison, the FWHM values determined for the 85.7° reflection of films grown in the $TiCl_4$-H_2O process at 430–600 °C were somewhat greater being around 0.1°.

Very low FWHM values of rocking curves (0.038°) had been reported also for TiO_2 films deposited on c-sapphire from TiI_4 and H_2O_2 [103] although only rutile phase had been believed to be formed in the latter films. Much higher values of the rocking curve widths, ranging from 0.6 to 0.8° in our studies, were determined for the films deposited on r-sapphire. Markedly greater scattering of the structure orientation was probably a reason for the absence of Pendellösung fringes in the XRD patterns of the films deposited on these substrates (Figure 6).

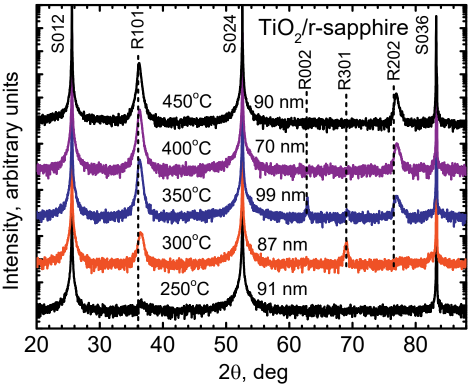

Figure 6. Symmetrical *θ–2θ scan diffraction patterns of films grown on* r-*sapphire at different temperatures using the* $TiCl_4$-O_3 *process [***IV***]. Vertical lines show reflection positions of rutile (R).*

Films deposited on r-sapphire substrates, contained mostly the (1 0 1) oriented rutile phase according to θ–2θ XRD (Figure 6.). However, in the diffraction patterns of the films deposited at 300 and 350 °C, the rutile orientations (3 0 1) and (0 0 1) were also observed. This result supported the Raman spectroscopy data about growth of rutile on r-sapphire at these temperatures and demonstrated that the $TiCl_4$-O_3 process allowed deposition of rutile on r-sapphire at relatively low temperatures [**II**]. It can be seen in Figure 6 that the rutile reflections observed were shifted to larger 2θ values compared to those of the ICDD 78-2485 database, particularly in the case of films deposited at 400–500 °C. The distance between (1 0 1) planes calculated for the films deposited at 350 °C was 0.2476 nm, i.e. about 0.4% smaller than the database value of rutile. With the increase of T_G to 425 °C, the difference increased to 1% and then, with the further increase of T_G to 600 °C, gradually decreased to 0.2%. Thus, there was evidently a strain in the films while the strain markedly depended on T_G.

Accordingly, the standard symmetrical HRXRD was not sufficient to confirm the presence of TiO_2-II in epitaxial films grown on c-sapphire, as appearance of reflections at slightly different angles compared to those of rutile could also be caused by mechanical stresses in the films. For this reason, to unambiguously determine the presence of TiO_2-II and characterize the in-plane orientation of crystallites, *φ*-scans for the reflections from the (0 2 –2 10) plane of sapphire (S (0 2 –2 10)), (3 0 1) plane of rutile (R (3 0 1)), and (3 1 1) plane of TiO_2-II (II (3 1 1)) were recorded [**I**,**II**]. The *φ*-scan involves rotating the sample around an axis perpendicular to the surface of the sample while keeping the incident and diffracted beam angles fixed. For R (3 0 1), six reflections were observed, while in the case of II (3 1 1), there were 12 reflections (Figure 7). Comparing the scans, the following in-plane epitaxial relationships were determined for coexisting TiO_2-II and rutile: $[0\,\bar{1}\,0]_{\mathrm{II}} \parallel [0\,1\,\bar{1}\,0]_{\mathrm{S}}$, $[0\,0\,1]_{\mathrm{II}} \parallel [2\,\bar{1}\,\bar{1}\,0]_{\mathrm{S}}$ for TiO_2-II and sapphire, and $[0\,1\,0]_{\mathrm{R}} \parallel [2\,\bar{1}\,\bar{1}\,0]_{\mathrm{S}}$, $[0\,0\,1]_{\mathrm{R}} \parallel [0\,1\,\bar{1}\,0]_{\mathrm{S}}$ for rutile and sapphire [**I**–**III**].

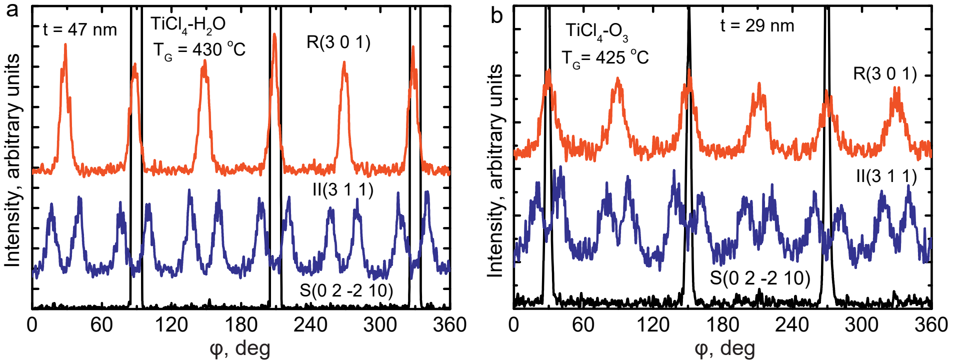

*Figure 7. φ-scans of the films grown in (a) the $TiCl_4$-H_2O process [**I**] and (b) the $TiCl_4$-O_3 process [**II**]. R, II and S denote the crystallographic planes of the rutile, TiO_2-II and substrate respectively.*

In addition, in-plane XRD analysis of reflections 0 2 0, 0 0 2 of TiO_2-II and 0 1 1 of rutile, reciprocal space maps (RSM) for the reflection 3 1 1 of TiO_2-II and 3 1 0, 3 0 1 reflections of rutile were measured to determine both out-of-plane and in-plane lattice parameters of TiO_2-II and rutile [**I**,**II**]. The unit cell parameters, determined for TiO_2-II deposited at 425 °C on c-sapphire from $TiCl_4$ and O_3 were a_{II} = 4.531 Å, b_{II} = 5.47 Å, and c_{II} = 4.75 Å [**II**]. In a recent study, Campanale *et al.* [124] reported the unit cell parameters of TiO_2-II to be a_{II} = 4.547 Å, b_{II} = 5.481 Å, and c_{II} = 4.891 Å. Therefore, in the films deposited on c-sapphire, the lattice of TiO_2-II was compressed by approximately 0.2% in the [0 1 0] direction and 2.9% in the [0 0 1] direction. For comparison, the lattice of rutile, formed in these films, was expanded by 2.9% in the [0 1 0] direction and compressed by 2.0% in the [0 0 1] direction [**II**].

As discussed earlier, the lattice of rutile epitaxially grown on c-sapphire should be expanded by 3.7% in the [0 1 0] direction and compressed by 8.4% in the [0 0 1] direction [**I**]. Thus, the simultaneous formation of rutile and TiO_2-II instead of single-phase rutile leads to the reduction of strain. Campanale *et al.* [124] have suggested recently that a potential transition from rutile to TiO_2-II could occur due to the compression of the rutile unit cell in the direction [0 –1 1].

5.2 Growth rate, roughness and density

Figure 8 depicts the temperature dependencies of growth rates and surface roughness values for films grown on r- and c-sapphire using $TiCl_4$-H_2O and $TiCl_4$-O_3 ALD processes. The growth rate, presented as the thickness growth per cycle, was calculated as the ratio of film thickness to the number of cycles used for the film growth. The films were grown using 800–3000 ALD cycles. The thicknesses of films deposited from $TiCl_4$ and H_2O ranged from 48 to 60 nm on r-sapphire and from 46 to 100 nm on c-sapphire while the thicknesses of films deposited from $TiCl_4$ and O_3 were 23–55 nm on both substrates. It is observed that the growth rates of films deposited on c-sapphire at $T_G \geq 350$ °C were slightly lower in $TiCl_4$-H_2O process than those of films deposited using O_3 as the oxygen source. In the $TiCl_4$-H_2O process, the growth rate on c-sapphire decreased when the deposition temperature increased from 350 to 500 °C. With the further increase of T_G to 680 °C, the growth rate remained practically unchanged. In the T_G range of 430–500 °C, the growth rate of films grown on c-sapphire using the $TiCl_4$-H_2O process was lower than that of films grown on r-sapphire. The decrease in the growth rate on c-sapphire with the T_G increase from 350 to 500 °C could be associated with the formation of TiO_2-II in the films (Figures 2a and 5a). The growth rate of films grown on r-sapphire did not depend on T_G in the range of 350–430 °C but decreased when T_G increased from 430 to 680 °C. The minimum roughness of films grown using $TiCl_4$ and H_2O as the precursors was approximately 1.0–1.9 nm on r-sapphire and 2.0–2.5 nm on c-sapphire in the temperature range of 350–500 °C. These roughness values were approximately twice as much as those of films deposited using O_3 as the oxygen source (Figure 8b).

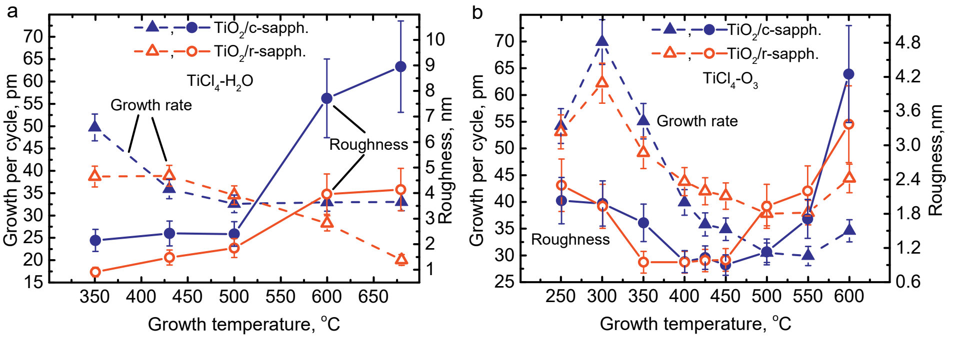

Figure 8. Dependence of growth per cycle and surface roughness on growth temperature of films deposited in (a) $TiCl_4$-H_2O and (b) $TiCl_4$-O_3 processes.

Figure 8b illustrates that at $T_G \leq 350$ °C, the growth from $TiCl_4$ and O_3 was faster on c-sapphire than on r-sapphire. With increasing T_G, the growth rate on c-sapphire decreased rapidly and became lower than that on r-sapphire. Based on the structural studies, it can be concluded that with the T_G increase to 450 V, the content of TiO_2-II formed in the films deposited on c-sapphire significantly increased (Figures 2b and 5b) whereas no considerable changes in the phase composition was observed on r-sapphire where rutile was predominantly formed at $T_G \geq 350$ °C. Therefore, it can be assumed that in the $TiCl_4$-O_3 process, the growth of the TiO_2-II phase was slower than that of rutile.

At T_G of 350–450 °C and 400–500 °C used for ALD of films on r- and c-sapphire, respectively, the films with the lowest surface roughness values (~1 nm) were obtained in the $TiCl_4$-O_3 process. Another difference between the two deposition processes was that the roughness of films grown on r-sapphire in the $TiCl_4$-H_2O process was significantly lower than that of the films grown on c-sapphire.

When the growth temperature increased above 500 °C, the surface roughness as well as growth rate of the films grown in the $TiCl_4$-O_3 process started to increase (Figure 8b). Since the surface roughness of the films grown on both r- and c-sapphire also increased, it can be assumed that the corresponding increase in the growth rate at higher T_G could, at least in some extent, be caused by the increase in the surface roughness. The surface roughness of the films grown from $TiCl_4$ and H_2O on c-sapphire also increased with the T_G increase from 500 to 680 °C, while the growth rate practically remained unchanged or changed very little (Figure 8a). At the same time the corresponding increase in the surface roughness of films grown on r-sapphire was much smaller. Thus, it is likely that these differences in the surface roughness could also contribute to the increasing difference between the growth rates on c- and r- sapphire (Figure 8a).

The roughness increase, observed with the T_G increase from 450–500 °C to 600 °C was evidently related to the surface roughening in the beginning of deposition, as it was revealed by AFM studies [**II**]. For instance, surface roughness values as high as 1.6–2.6 nm were measured for the films with thicknesses below 10 nm grown at 600 °C in the $TiCl_4$-O_3 process [**II**]. These roughness values considerably exceed those of the films deposited on r-sapphire at 350–450 °C and on c-sapphire at 400–500 °C (Figure 8).

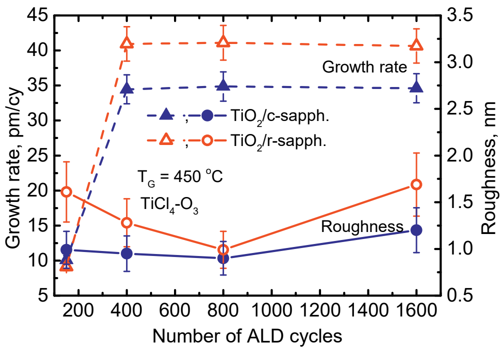

Figure 9. Dependence of growth per cycle and surface roughness on the number of ALD cycles used for deposition of films in the $TiCl_4$-O_3 process at 450 °C.

Figure 9 shows the dependence of GPC and surface roughness on the number of ALD cycles used for deposition of films at 450 °C. The film thicknesses ranged from 2.9 to 69 nm and from 3.3 to 65 nm on c- and r-sapphire substrates, respectively. GPC of the thinnest films grown with 150 ALD cycles was significantly lower than that of the films deposited with 400–1600 cycles. Therefore, in the initial stage of deposition, the growth was hindered on both orientations of substrates. The GPC of films that were deposited using 400–1600 cycles depended on the substrate orientation as described earlier.

The surface roughness of the films grown on c-sapphire only a little depended on the number of ALD cycles and remained within the range of 1–1.2 nm. The surface roughness of films deposited on r-sapphire more significantly depended on the number of deposition cycles showing a minimum at 800 cycles where the roughness was close to that of films on c-sapphire. The roughness increase observed with the decrease in the number of cycles applied for deposition of films on r-sapphire can be explained by the island type of growth in the beginning of deposition. With the thickness increase, the islands grew together, and the roughness decreased.

Although the surface roughness of films deposited on c-sapphire did not increase with the decrease in the number of cycles, the surface roughness of films deposited with 150 cycles (1 nm) was relatively close to the mean thickness (2.9 nm) of these films. Furthermore, the crystallite sizes determined for these films were around 5 nm [**II**], that is, the crystallite sizes exceeded the film thickness. These results indicate that the film growth started with the formation of islands on c-sapphire as well. This explains why the growth was hindered in the beginning of deposition on both types of substrates.

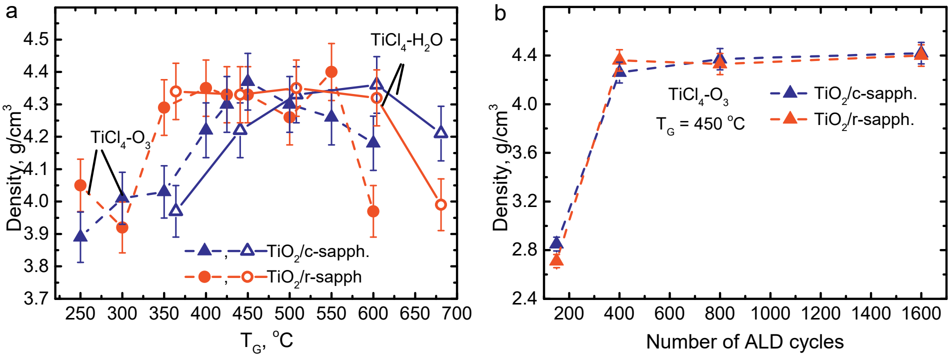

Figure 10. Dependence of density on (a) growth temperature and (b) the number of cycles applied for ALD of films at 450 °C.

The maximum densities of the films ranged from 4.2 to 4.4 g/cm^3, being comparable to the theoretical densities of the rutile and TiO_2-II (ICDD PDF-2 database cards 78-1286 and 01-076-6065, respectively). Such values were reached for films grown on both r-sapphire and c-sapphire. The most significant changes and differences in the densities were observed in a T_G range of 250–450 °C and at

$T_G \geq 600$ °C (Figure 10a). On r-sapphire, the density increased to 4.3 g/cm^3 with the T_G increase to 350 °C (Figure 10a). According to Raman spectroscopy and X-ray diffraction data [**II**], this increase in the density was related to the increase in the rutile and decrease in the anatase content in the films. On c-sapphire, densities began to increase markedly, when T_G exceeded 350 °C in both the $TiCl_4$-O_3 and $TiCl_4$-H_2O processes. In both cases, the increase in the density correlates well with the formation of the TiO_2-II phase in the films (Figures 2 and 5). Therefore, it can be concluded that these changes in the densities are due to the phase composition changes in the films. In contrast, the decrease in the densities that appeared with the T_G increase from 500–550 to 600 °C in the $TiCl_4$-O_3 process and from 600 to 680 °C in the $TiCl_4$-H_2O process was probably caused by the decreasing homogeneity of the film structure leading to the increase in the surface roughness as well (Figure 8).

The dependence of density on the number of growth cycles used for deposition of films from $TiCl_4$ and O_3 at 450 °C is shown in Figure 10b. The densities of the thinnest films (with thicknesses of 2.9–3.2 nm), grown with 150 cycles, ranged from 2.71–2.85 g/cm^3, being significantly lower than the densities of thicker films. Low densities of the former films can be explained by the island growth in the beginning of deposition. The surface roughness of these films (Figure 9), which is comparable to the film thicknesses, also indicates the island growth. The densities of thicker films, remaining in the range of 4.26–4.4 g/cm^3, depended very little on the number of cycles and, thus, on the film thicknesses.

5.3 Optical properties

In order to characterize optical properties of films, containing TiO_2-II, and compare the properties of these films with those of anatase and rutile, films grown from $TiCl_4$ and O_3 at temperatures of 250–450 °C on c- and r-sapphire and SiO_2 substrates were studied. Figure 11 presents the results of spectrophotometry (SPM) studies, that is, the transmission (Figure 11a) and reflection (Figure 11b) spectra for films grown on these substrates at 450 °C. The spectra of films that are thicker than 55 nm display interference fringes, influenced by the film thicknesses, refractive indices, and absorption coefficients [125]. Thinner films more distinctly show the fringe extremes only in the reflection spectra (Figure 11b) due to the appearance of the fringes in the regions of medium and strong absorption where the transmission oscillations are less noticeable (Figure 11a). Notably, the films measuring 55–101 nm in thickness exhibit transmission maxima and reflection minima that match the baseline values of uncoated substrates at corresponding wavelengths, suggesting minimal impact from absorption, diffuse transmission, and/or diffuse reflection [**III**].

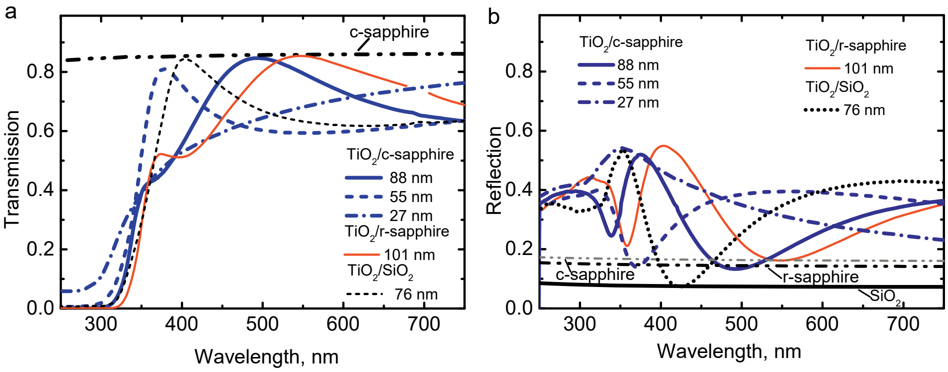

Figure 11. (a) Transmission and (b) reflection spectra of TiO_2 *films with different thicknesses deposited on sapphire and* SiO_2 *substrates [**III**]. Transmission and reflection spectra of substrates are depicted for comparison.*

Absorption spectra (Figure 12) were derived using an approximation $\alpha = (1/t)\ln((1-R)/T)$ that was based on transmission (T) and reflection (R) coefficients [126]. The film thickness, used in this formula, was measured by XRR in our experiments. This method for calculation of absorption coefficient aligns well with alternative complex methods, such as direct inversion of Fresnel's equations, especially at lower absorption coefficient values. However, it slightly overestimates α values, with inaccuracies within 5–10%, comparable to experimental errors [126]. The spectra show that the crystal structure significantly influences the absorption spectra of films (Figure 12). For instance, rutile films that grew on r-sapphire display more significant increase in absorption at lower photon energies ($h\nu$) compared to the films grown on c-sapphire and SiO_2 (Figure 12). In contrast, anatase films consistently show a spectral feature at around 3.9 eV, typical of electron transitions specific to the energy band structure of anatase [127].

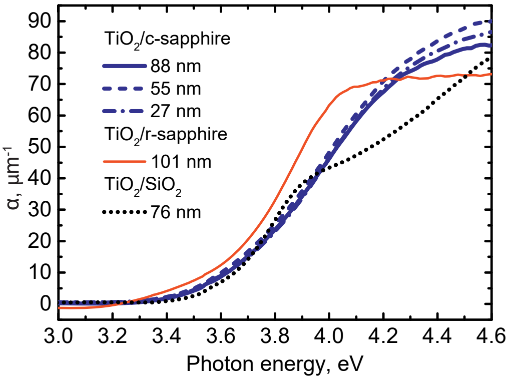

Figure 12. Absorption spectra of TiO_2 *films deposited on sapphire and* SiO_2 *substrates [**III**].*

The results, shown in Figure 13, indicate that the refractive index values of films deposited on identical substrates varied only a little with marked variation of the film thickness. However, the type of substrate and, accordingly, the crystalline phases present in the films significantly influenced the refractive indices (Figure 13, Table 4). Films containing the TiO_2-II phase exhibited higher *n* values at photon energies up to 2.75 eV. For example, at 2.48 eV, the *n* values were 2.60 ± 0.03 for anatase, 2.74 ± 0.04 for rutile, and 2.80 ± 0.04 for TiO_2-II-rich films. At 1.96 eV, these values were 2.48 ± 0.04, 2.62 ± 0.04, and 2.67 ± 0.03, respectively. At the photon energies above 2.75 eV, the refractive indices of rutile and TiO_2-II films converged due to the steeper increase in the refractive index of rutile at higher photon energies, possibly due to narrower band gap of rutile compared to that of TiO_2-II [**III**].

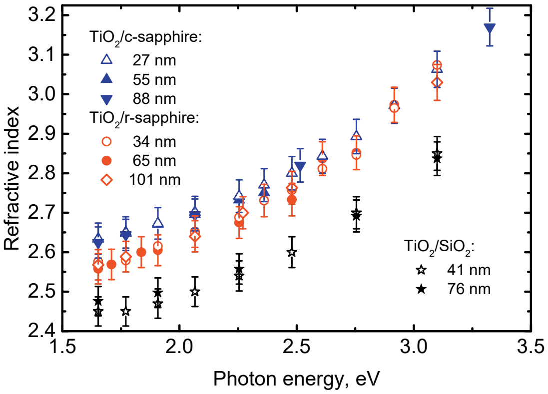

*Figure 13. Refractive index dispersion curves of TiO_2 films with different thicknesses deposited on c-sapphire, r-sapphire and SiO_2 substrates [**III**].*

Expectedly, the anatase films showed lower *n* values compared to those of rutile and TiO_2-II across the photon energy studied in this research (Figure 13). Refractive indices measured by spectroscopic ellipsometry (SE) were consistent with those obtained from the SPM data, reinforcing the reliability of the findings. At 1.96 eV, that is at a wavelength of 633 nm, ellipsometry yielded mean *n* values of 2.49 ± 0.03 for anatase, 2.57 ± 0.03 for rutile, and 2.61 ± 0.03 for TiO_2-II/rutile, corresponding to films deposited on SiO_2, r-sapphire, and c-sapphire substrates, respectively [**III**]. Assuming that the intensity of the Raman band correlates with the quantity of material responsible for Raman scattering, it can be inferred that the concentration of rutile did not surpass 10% in the films deposited on c-sapphire at T_G = 450 °C using the $TiCl_4$-O_3 process [**III**]. Thus, the refractive index values of these films should be close that of TiO_2-II.

The refractive indices measured at λ = 633 nm for the films deposited on c-sapphire substrates were found to be dependent on the deposition temperature (Table 4). Notably, the *n* values of the TiO_2-II/rutile films grown on c-sapphire at temperatures ranging from 400 to 450°C were slightly elevated compared to the refractive indices of rutile films grown on r-sapphire under similar temperature conditions (Table 4). A surprising observation emerged was a decrease in the refractive indices of rutile films deposited on r-sapphire with increasing T_G from 250 to 400–450 °C (Figure 10d of Ref. **IV**). This unexpected trend could be attributed to the optical anisotropy of rutile [128,129] and the alterations in crystallite orientations with the change of T_G (Figure 6). Indeed, as can be seen in Figures 4a and 6, films containing poorly developed rutile with inclusions of anatase were obtained on r-sapphire at 250 °C. At 300–350 °C, rutile containing crystallites with orientations (1 0 1), (0 0 2), and (3 0 1) as well as minor traces of anatase were formed while at 400–450 °C, rutile with (1 0 1) orientation grew on r-sapphire.

Table 4. Refractive indices determined at a wavelength of 633 nm by spectrophotometry and spectroscopic ellipsometry methods for TiO_2 thin films deposited on SiO_2, c-sapphire and r-sapphire substrates at different temperatures.

Substrate	***t*, nm**	**T_G, °C**	**Phase***	**Refractive index**	**Measurement method**	**Reference**
SiO_2	90	250	A	2.48 ± 0.03	SE	IV
SiO_2	105	350	A	2.49 ± 0.03	SE	IV
SiO_2	41	450	A	2.44 ± 0.04	SPM	III
SiO_2	76	450	A	2.49 ± 0.04	SPM	III
SiO_2	103	450	A + R	2.52 ± 0.03	SE	IV
SiO_2	111	450	A +R	2.48 ± 0.04	SPM	III
c-sapphire	106	250	A	2.49 ± 0.03	SE	IV
c-sapphire	120	350	A	2.50 ± 0.03	SE	IV
c-sapphire	103	400	A + II + R	2.63 ± 0.03	SE	IV
c-sapphire	27	450	II + R	2.67 ± 0.04	SPM	III
c-sapphire	55	450	II + R	2.67 ± 0.04	SPM	III
c-sapphire	88	450	II + R	2.67 ± 0.04	SPM	III
c-sapphire	88	450	A + II + R	2.64 ± 0.03	SE	IV
r-sapphire	91	250	R	2.68 ± 0.03	SE	IV
r-sapphire	99	350	R	2.67 ± 0.03	SE	IV
r-sapphire	70	400	R	2.59 ± 0.03	SE	IV
r-sapphire	34	450	R	2.63 ± 0.04	SPM	III
r-sapphire	65	450	R	2.62 ± 0.04	SPM	III
r-sapphire	90	450	R	2.59 ± 0.03	SE	IV
r-sapphire	101	450	R	2.62 ± 0.04	SPM	III

* A – anatase, R – rutile, II –TiO_2-II

The optical bandgap energies of the films that were deposited on c-sapphire and contained the TiO_2-II phase were notably higher than those of rutile but slightly lower than E_g of anatase films, as listed in Table 5. The difference between the E_g values of the anatase films and those of the films containing TiO_2-II that was around 0.06 did not exceed the experimental uncertainty. However, this difference aligns closely with the shift in the absorption spectrum of about 0.07 eV determined in high-pressure experiments of Ohta et al [112] during a pressure-induced phase transition from anatase to TiO_2-II at pressures ranging from 3.9 to 4.2 GPa.

The optical bandgaps of the anatase films that were grown on c-sapphire at 250–350 °C were similar to those deposited on SiO_2 substrates at the same temperatures (Table 5). Somewhat lower bandgap energy of 3.22 eV was determined for the films deposited on c-sapphire at $T_G = 400$ °C. This temperature is close to the lowest T_G allowing formation of significant TiO_2-II/rutile amounts in the films. However, even these reduced bandgap values remained considerably higher than those observed for films containing only rutile (Table 5). The results presented here align well with the recent publication by Gordeeva *et al.* [130]. In their report, they determined bandgap values for anatase, rutile, and TiO_2-II, which were found to be 3.20–3.40 eV, 2.99–3.09 eV, and 3.18–3.45 eV, respectively [130].

Table 5. Optical bandgap values determined from spectrophotometry data for TiO_2 thin films deposited on SiO_2, c-sapphire and r-sapphire substrates.

Substrate	***t*, nm**	**T_G, °C**	**Phase***	**Bandgap, eV**	**Reference**
SiO_2	90	250	A	3.25 ± 0.03	[IV]
SiO_2	105	350	A	3.31 ± 0.03	[IV]
SiO_2	41	450	A	3.36 ± 0.09	[III]
SiO_2	76	450	A	3.39± 0.09	[III]
SiO_2	103	450	A + R	3.28 ± 0.03	[IV]
SiO_2	111	450	A + R	3.00 ± 0.08	[III]
c-sapphire	106	250	A	3.28± 0.03	[IV]
c-sapphire	120	350	A	3.28 ± 0.03	[IV]
c-sapphire	103	400	A + II + R	3.22 ± 0.03	[IV]
c-sapphire	27	450	II + R	3.36 ± 0.09	[III]
c-sapphire	55	450	II + R	3.32 ± 0.09	[III]
c-sapphire	88	450	II + R	3.28 ± 0.08	[III]
c-sapphire	88	450	A + II + R	3.24 ± 0.03	[IV]
r-sapphire	91	250	R	3.11 ± 0.03	[IV]
r-sapphire	99	350	R	3.13 ± 0.03	[IV]
r-sapphire	70	400	R	3.09 ± 0.03	[IV]
r-sapphire	34	450	R	3.16 ± 0.09	[III]
r-sapphire	65	450	R	3.06 ± 0.06	[III]
r-sapphire	90	450	R	3.08 ± 0.03	[IV]
r-sapphire	101	450	R	3.08 ± 0.05	[III]

* A – anatase, R – rutile, II – TiO_2-II

5.4 Mechanical properties

The hardness, as determined by nanoindentation (Figure 14), depended on the phase composition of the films. The films that were deposited on r-sapphire at 250 °C and contained rutile and minor amounts of anatase exhibited the highest hardness values, ranging from 17.0 to 17.5 GPa at tip displacements of 15–20 nm (Figure 14a). Similarly, high values were recorded for films deposited on c-sapphire at 400–450 °C (Figure 14b). In contrast, the rutile films deposited at 450 °C on r-sapphire showed notably lower hardness values, ranging between 15.2 and 15.5 GPa. The observed decrease in hardness at higher T_G is likely linked to the increase in crystallite sizes and variations in crystallite orientations, as discussed by Kulikovsky et al. [131].

Considering the data of the XRD analysis, the mean crystallite sizes were as small as 9 nm in the rutile films deposited on r-sapphire at 300 °C (Figure 7 of Ref. **IV**) and probably even smaller in the films grown at 250 °C that contained poorly developed rutile according to XRD data presented in Figure 6 and some inclusions of anatase according to the Raman spectroscopy results depicted in Figure 4a. As a result, the high hardness values observed can be explained by formation of a nanocrystalline composite containing different phases.

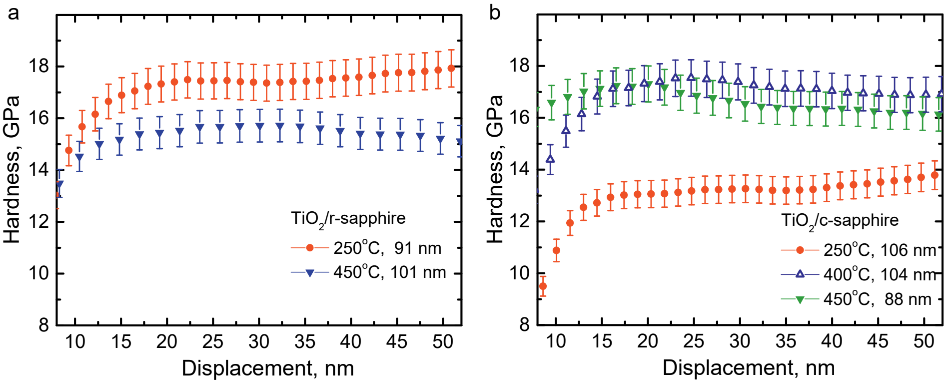

*Figure 14. Hardness as a function of tip displacement recorded for TiO_2 films grown at different temperatures on (a) r- and (b) c-sapphire [**IV**].*

Crystallite sizes determined for rutile films grown at 450 °C were 23 nm while the hardness values of 15.5 GPa at tip displacement 20 nm were markedly smaller than those measured for films deposited on r-sapphire at 250 °C [**IV**]. Similar decrease in hardness with increasing crystallite sizes was reported for rutile films deposited by magnetron sputtering [131].

The lowest hardness values (around 13 GPa) were measured in this work for films containing anatase phase (Figure 14). Lower hardness of anatase compared to that of rutile is consistent with earlier findings [131]. However, the hardness values determined for anatase by Kulikovsky et al. [131] are somewhat lower than those of our anatase films grown at 250 °C on c-sapphire. For comparison, Ylivaara et al. [132] reported hardness values of 10.5–13.6 GPa and crystallite sizes of 24–27 nm for anatase films that were grown by ALD on silicon substrates at 250–300 °C. Thus, the highest values published by Ylivaara et al. [132] are close to the hardness of our anatase films. Notably, the crystallite sizes in these two sets of anatase films were also comparable to each other as the XRD crystallite sizes determined for our anatase films grown at 250 °C on c-sapphire were 18–22 nm (Figure7 of Ref. **IV**). These results suggest that the phase composition significantly influence the mechanical characteristics of the films [**IV**]. Comparing the hardness values (Figure 14) and crystallites sizes of 23 and 80–95 nm determined for films deposited at 450 °C on c- and r-sapphire, respectively (Figure 7 of Ref. **IV**), and considering that the decrease in crystallite sizes should lead to an increase in hardness, one can conclude that at similar crystallite sizes the hardness of TiO_2-II and/or mixed TiO_2-II/rutile phases is higher than that of pure rutile and mixed rutile and anatase phases.

SUMMARY AND CONCLUSIONS

The results of structural studies conducted in this research demonstrate that TiO_2 films grew epitaxially on both c- and r-sapphire. The phase composition of TiO_2 films depended on the orientation of substrates, growth temperature, process time parameters, and film thicknesses. Films deposited on c-sapphire substrates contained the mixture of anatase, rutile, and high-pressure TiO_2-II, when the films were grown at temperatures of 350–430 °C, and the mixture of (1 0 0) oriented rutile and TiO_2-II, when the films were grown from $TiCl_4$ and H_2O at 475–680 °C and from $TiCl_4$ and O_3 at 450–600 °C. It was also determined in these studies that standard symmetrical HRXRD was not sufficient to identify the presence of TiO_2-II in epitaxial films grown on c-sapphire, as appearance of reflections at slightly different angles compared to those of rutile reflections could also be caused by mechanical stresses in the films. Therefore, the conclusions about the presence of TiO_2-II in the films was mainly based on Raman spectroscopy and non-coplanar XRD analyses. Based on the latter analysis,the in-plane epitaxial relationships were determined to be $[0\,\bar{1}\,0]_{\mathrm{II}} \parallel [0\,1\,\bar{1}\,0]_{\mathrm{S}}$ and $[0\,0\,1]_{\mathrm{II}} \parallel [2\,\bar{1}\,\bar{1}\,0]_{\mathrm{S}}$ for TiO_2-II and sapphire, and $[0\,1\,0]_{\mathrm{R}} \parallel [2\,\bar{1}\,\bar{1}\,0]_{\mathrm{S}}$ and $[0\,0\,1]_{\mathrm{R}} \parallel [0\,1\,\bar{1}\,0]_{\mathrm{S}}$ for rutile and sapphire.

At deposition temperatures exceeding 500 °C, the content of TiO_2-II in the films began to decrease with increasing deposition temperature. However, at all temperatures that were used for comparison of different ALD processes, TiO_2-II was more preferentially formed in the $TiCl_4$-O_3 process than in the $TiCl_4$-H_2O process. With the increasing film thickness, the content of TiO_2-II decreased while that of rutile increased. In the case of $TiCl_4$-H_2O process, the relative amount of TiO_2-II phase increased with increasing $TiCl_4$ exposure time. The films grown at 350 °C in the $TiCl_4$-O_3 process showed that the decrease in the O_3 pulse duration and increase in the $TiCl_4$ pulse and the first purge durations caused an increase in the relative amount of TiO_2-II in the films. Unfortunately, the ALD process time parameters that favored the growth of TiO_2-II at 350 °C, inhibited the formation of this phase compared to that of rutile at 500 °C. Thus, the optimization of the time parameters allowed for lowering the temperatures, promoting the most efficient growth of TiO_2-II, yet it did not significantly broaden the temperature range enabling the preferential growth of this phase.

In contrast, the films deposited from $TiCl_4$ and O_3 on r-sapphire substrates at $T_G \geq 400$ °C consisted of (1 0 1)-oriented epitaxial rutile whereas the films grown on these substrates at 300–350 °C contained (1 0 1), (0 0 1), and (3 0 1) oriented rutile. For comparison, in the films grown on amorphous SiO_2 substrates at 250–450 °C, only the anatase phase or anatase with traces of rutile were observed. Therefore, the appropriate choice of a crystalline substrate and its orientation enabled us to control the phase composition of TiO_2 films grown by ALD in the $TiCl_4$-H_2O and $TiCl_4$-O_3 processes. Most importantly, due to epitaxial growth, it was possible to deposit films on c-sapphire where TiO_2-II was the dominant phase.

The growth rate depended on the deposition temperature and oxygen precursor as well as on the phase composition of films. The densities of films, which were deposited on sapphire substrates, reached 4.2–4.4 g/cm^3 being comparable to the theoretical densities of the rutile and TiO_2-II phases. These results, as well as the Pendellösung fringes observed in the HRXRD patterns of films with high content of TiO_2-II confirmed that the crystalline quality of these films was high.

Notably, using the $TiCl_4$-H_2O and $TiCl_4$-O_3 ALD processes, it was possible to obtain relatively thick films with low surface roughness on both c- and r-sapphire. This allowed for reliable measurement of optical properties and hardness of these films. The refractive index values of the TiO_2-II/rutile films grown on c-sapphire at temperatures ranging from 400 to 450 °C were slightly elevated compared to the refractive indices of rutile films grown on r-sapphire at similar temperatures while across the wavelength range studied in this work, the anatase films showed markedly lower refractive index values compared to those containing rutile and TiO_2-II.

The optical bandgap energies of 55–103 nm thick films that were deposited on c-sapphire and contained the TiO_2-II phase ranged from 3.22 to 3.32 eV being notably higher than those of rutile films with similar thicknesses (3.06–3.09 eV for 65–101 nm thick films) grown at 400–450 °C on r-sapphire. The optical bandgap energies, determined for the films grown on c-sapphire at 250 °C and on SiO_2 at 250–450 °C ranged from 3.25 to 3.39 eV. Hence, the optical bandgap of TiO_2-II is narrower than that of anatase, which may be one reason why TiO_2-II is a more effective photocatalyst than anatase.

The hardness values depended on the phase composition and crystallite sizes. The films that were deposited on r-sapphire at 250 °C and contained rutile with mean XRD crystallite sizes < 9 nm and minor amounts of anatase exhibited the highest hardness values, ranging from 17.0 to 17.5 GPa at tip displacements of 15–20 nm. Similar results were obtained for TiO_2-II/rutile films grown on c-sapphire at substrate temperatures of 450 °C. However, the crystallite sizes were markedly higher in the latter films than in the former ones. Considering that the increase in crystallite sizes caused a noticeable decrease in the hardness of rutile films, one can conclude that at similar crystallite sizes, the hardness of TiO_2-II and/or mixed TiO_2-II/rutile phases are higher than those of pure rutile and mixed rutile/anatase phases.

In conclusion, the results of this work provide some insights into the possibilities to obtain and stabilize the high-pressure metastable TiO_2-II phase in thin films and data on the effect of phase composition on optical and mechanical properties of films containing this phase. This information offers a basis for further exploration and potential for applications of TiO_2-II, for instance, in photocatalysis, optical devices, and functional coatings with enhanced hardness.

SUMMARY IN ESTONIAN

Metastabiilne TiO_2-II aatomkihtsadestatud õhukestes ja üliõhukestes kiledes: stabiliseerimine, omadused ja mõju kilede kasvule

Käesolevas töös uuriti TiO_2 kilesid, mis olid aatomkihtsadestamise meetodil kasvatatud erinevatele alustele. Aatomkihtsadestamise lähteaineteks olid aluse temperatuuridel 350–680 °C $TiCl_4$ ja H_2O ning temperatuuridel 250–600 °C $TiCl_4$ ja O_3. Uuritud kilede paksused jäid vahemikku 2,9–120 nm. Kilede kasvujärgseks uurimiseks kasutati ramanspektrokoopiat, röntgenpeegeldust, röntgendifraktsioonanalüüsi, spektrofotomeetriat, ellipsomeetriat ja nanoindenteerimise meetodit.

Struktuuriuuringud näitasid, et nii c- kui ka r-safiirile kasvasid kiled epitaksiaalselt. TiO_2 kilede faasikoostis sõltus kasvualusest, kasvutemperatuurist, kasvatusprotsessi tsükliaegadest ja kilede paksusest. C-safiirile sadestatud kiled sisaldasid segu anataasist, rutiilist ja titaandioksiidi kõrgrõhufaasist TiO_2-II, kui kiled olid kasvatatud temperatuuridel 350–430 °C, või (1 0 0) orientatsiooniga segu rutiilist ja TiO_2-II-st, kui kiled olid sadetatud temperatuuridel 475–680 °C $TiCl_4$-H_2O protsessis ja temperatuuridel 450–600 °C $TiCl_4$-O_3 protsessis. TiO_2-II orientatsioon aluse suhtes oli määratud epitaksiaalsuhetega $[0\,\bar{1}\,0]_{\mathrm{II}} \parallel [0\,1\,\bar{1}\,0]_{\mathrm{S}}$ ja $[0\,0\,1]_{\mathrm{II}} \parallel [2\,\bar{1}\,\bar{1}\,0]_{\mathrm{S}}$ ning rutiili orientatsioon aluse suhtes epitaksiaalsuhetega $[0\,1\,0]_{\mathrm{R}} \parallel [2\,\bar{1}\,\bar{1}\,0]_{\mathrm{S}}$ ja $[0\,0\,1]_{\mathrm{R}} \parallel [0\,1\,\bar{1}\,0]_{\mathrm{S}}$.

Kui kiled olid sadestatud temperatuuridel, mis ületasid 500 °C, hakkas TiO_2-II osakaal nendes temperatuuri tõusuga vähenema, kusjuures kogu sadestustemperatuuride vahemikus oli $TiCl_4$-O_3 protsessis kasvatatud kiledes TiO_2-II suhteline sisaldus suurem ja selle vähenemine aeglasem kui $TiCl_4$-H_2O protsessis kasvatatud kiledes. TiO_2-II sisaldus vähenes ja rutiili osakaal suurenes kilede paksuse suurenemisel. Kilede sadestamisel kasutatud $TiCl_4$ pulsside pikendamine tõstis TiO_2-II faasi osakaalu $TiCl_4$-H_2O protsessis kasvatatud kiledes. Kui lähteaineteks olid $TiCl_4$ ja O_3, siis O_3 pulsside lühendamisel ning $TiCl_4$ pulsside ja nendele järgnevate puhastusaegade pikkuse suurendamisel TiO_2-II suhteline sisaldus suurenes, kui kasvutemperatuuriks oli 350 °C. Paraku protsessiaegade parameetrid, mis soodustasid TiO_2-II kasvu 350 °C juures, pärssisid selle faasi kasvu 500 °C juures. Siiski võimaldas tsükliaegade optimeerimine alandada sadestustemperatuure, mille juures TiO_2-II kasv oli eelistatud. See ei laiendanud aga oluliselt optimaalset temperatuurivahemikku TiO_2-II saamiseks.

Samas, r-safiirile kasvas temperatuuridel üle 400 °C (1 0 1) orientatsiooniga rutiil ja temperatuuridel 300–350 °C (1 0 1), (0 0 1) ja (3 0 1) orientatsioonidega rutiil. Võrdluseks temperatuuridel 250–450 °C amorfsetele SiO_2 alustele sünteesitud kiled sisaldasid kas ainult anataasi või lisaks anataasile ka väikestes kogustes rutiili. Seega, sobiva aluse ja kristallilise orientatsiooni valik lubas meil kontrollida aatomkihtsadestamise meetodil sünteesitud TiO_2 kilede struktuuri.

Titaandioksiidi kasvukiirus sõltus nii sadestustemperatuurist, hapniku lähteainest kui ka kilede faasikoostisest. Safiiralustele sadestatud kilede tihedused ulatusid 4,2–4,4 g/cm^3-ni. Suured tiheduse väärtused, mis küündisid rutiili ja

TiO_2-II struktuuriandmetest määratud tihedusteni, ning Pendellösungi efekti jälgitavus c-safiirile sadestatud kilede röntgen-difraktogrammides viitavad nende kilede kõrgele kvaliteedile.

Kuna uuringutes kasutatud aatomkihtsadestamise meetod lubas valmistada safiiralustele suhteliselt pakse ja väikese pinnakaredusega kilesid, osutus võimalikuks nende kilede optiliste omaduste ja kõvaduse määramine. Selgus, et c-safiirile 400–450 °C juures kasvatatud TiO_2-II/rutiili kilede murdumisnäitajad olid veidi suuremad kui samal temperatuuril r-safiirile kasvatatud rutiilikilede murdumisnäitajad. Samal ajal amorfsele SiO_2-le sadestatud anataasikilede murdumisnäitajad olid kogu uuritud lainepikkuste vahemikus tunduvalt väiksemad kui rutiili ja TiO_2-II sisaldavate kilede murdumisnäitajad.

C-safiirile kasvatatud 55–103 nm paksuste TiO_2-II sisaldusega kilede keelutsooni laiused jäid vahemikku 3.22–3.32 eV olles märkimisväärselt suuremad, kui r-safiirile temperatuuridel 400–450 °C kasvatatud 65–101 nm paksuste rutiilkilede keelutsoonilaiused, mis jäid vahemikku 3.06–3.09 eV. Kasvutemperatuuridel 250 °C ja 250–450 °C, vastavalt c-safiirile ja SiO_2-le kasvatatud anataaskilede keelutsoonilaiused olid 3.25–3.39 eV. Seega TiO_2-II suhteliselt suur fotokatalüütiline efektiivsus, millest on kirjanduses teada antud, võib vähemalt osaliselt olla tingitud TiO_2-II kitsamast keelutsoonist võrreldes anataasi keelutsooniga.

Kilede kõvadused sõltusid faasikoostisest ja kristalliitide suurustest. Kiledel, mis olid kasvatatud r-safiirile 250 °C juures ning c-safiirile 400–450 °C juures ja mis sisaldasid vastavalt vähese anataasilisandiga rutiili ning segu rutiilist ja TiO_2-II-st, olid suurimad kõvaduse väärtused, mis ulatusid 17,0–17,5 GPa-ni. Arvestades aga kristalliitide suuruste erinevust erineva faasikoostisega kiledes ning teiselt poolt kristalliitide suuruse mõju kilede kõvadusele, oli võimalik järeldada, et ühesuguse kristalliitide suuruse korral, peaksid TiO_2-II sisaldavad kiled olema suurema kõvadusega kui rutiili ja anataasi sisaldavad kiled.

ACKNOWLEDGEMENTS

I would like to express my deepest appreciation to all those who provided me the possibility to complete this thesis. A special gratitude I give to my supervisors, Prof. Jaan Aarik and Dr. Hugo Mändar, whose suggestions and encouragement, helped me to coordinate my studies and writing this thesis. Their guidance, support, patience, and immense knowledge helped me in my research.

Besides my supervisors, I would like to thank Aivar Tarre and Lauri Aarik for their comprehensive assistance, insightful comments, encouragement and especially for their answers to all my questions.

I would also like to extend my thanks to Aarne Kasikov, Taivo Jõgiaas, Ahti Niilisk and Peeter Ristlaid for their assistance in conducting measurement experiments and to Alma-Asta Kiisler for her kind words and assistance in the substrate preparation.

I am deeply grateful to my family who not only supported and encouraged me to strive towards my goal, but also showed understanding and patience, providing me the time needed to complete my studies. Additionally, I would like to express my gratitude to my team at KSVEE for their support and encouragement.

REFERENCES

[1] F. Parrino, L. Palmisano, Titanium Dioxide (TiO_2) and its applcations, *Elsevier*, 2020.

[2] D. Rathee, S. K. Arya, M. Kumar, Analysis of TiO_2 for microelectronic applications: effect of deposition methods on their electrical properties, *Front. Optoelectron.* 4 (2012), 349–358.

[3] K. Nakata, A. Fujishima, TiO_2 photocatalysis: Design and applications, *JPPC* 13 (3) (2012) 169–189.

[4] A. J. Haider, Z. N. Jameel, I. H. M. Al-Hussaini, Review on: Titanium Dioxide Applications, *Energi Procedia* 157 (2019) 17–29.

[5] V. Cremers, R. L. Puurunen, J. Dendooven, Conformality in atomic layer deposition: Current status overview of analysis and modelling, *Appl. Phys. Rev.* 6, (2019) 021302.

[6] J. Aarik, A. Aidla, H. Mändar, T. Uustare, M. Schuisky, A. Hårsta, Atomic layer growth of epitaxial TiO_2 thin films from $TiCl_4$ and H_2O on α-Al_2O_3 substrates, *J. Cryst. Growth* 242 (2002) 189–198.

[7] N. A. Drubovinskaia, L. S. Dubrovinsky, R. Ahuja, V. B. Prokopenko, A. Dimitriev, H. P. Weber, J. M. Osorio-Guillen, B. Johansson, Experimental and theoretical identification of a new high-pressure TiO_2 polymorph, *Phys. Rev. Lett.* 87 (27) (2001) 275501.

[8] R. Ahuja, L. S. Dubrovinsky, Cotunnite-structured titanium dioxide and the hardest known oxide, *High Pressure Res.* 22 (2022) 429–433.

[9] X. Wu, W. Holbig, G. Steinle-Neumann, Structural Stability of TiO_2 at high pressure in density functional theory based calculations, *J. Phys.: Condens. Matter* 22 (2010) 295501.

[10] A. E. Goresy, M. Chen, P. Gillet, L. Dubrovinsky, G. Graup, R. Ahuja, A natural shock-indused dense polymorph of of rutile with α-PbO_2 structure in te suevite from the Ries crater in Germany, *Earth. Planet. Sci. Lett.* 192 (2001) 485–495.

[11] T. I. Dyuzheva, L. M. Lityagina, N. A. Bendeliani, Hydrothermal crystal growth of the high-pressure phases of α-PbO_2 and TiO_2 II, *J. Alloys Compd.* 377 (2004) 17–20.

[12] L. Gerward, J. S. Olsen, Post-rutile high-pressure phases in TiO_2, *J. Appl. Cryst.* 30 (1997) 259–264.

[13] S. L. Hwang, P. Shen, H. T. Chu, T. F. Yui, Nanometer-size α-PbO_2-type TiO_2 in garnet: a thermobarometer for ultrahigh-pressure metamorphism, *Science* 288 (2000) 321–324.

[14] X. Wu, D. Meng, Y. Han, α-PbO_2-type nanophase of TiO_2 from coesite-bearing eclogite in the Dabie Mountains, China, *Am. Mineral.* 90 (2005) 1458–1461.

[15] D. Meng, X. Wu, X. Fan, Z. Zhang, H. Chen, X. Meng, J. Zheng, High pressure response of rutile polymorphs and its significanse for indicating the subduction depth of continental crust, *Acta Geol. Sinica* 82 (2) (2008) 371–376.

[16] Z. G. Mei, Y. Wang, S. L. Shang, Z. K. Liu, First-principles study of lattice dynamics and thermodynamics of TiO_2 polymorphs, *Inorg. Chem.* 50 (2011) 6996–7003.

[17] J. K. Dewhurst, J. E. Lowther, High-pressure structural phases of titanium dioxide, *Phys. Rev. B* 54 (6) (1996) R3673–R3675.

[18] J. Staun Olsen, L. Gerward, J. Z. Jiang, On the rutile/α-PbO_2-type phase boundary of TiO_2, *J. Phys. Chem. Solids* 60 (1999) 229–233.

[19] J. Muscat, V. Swamy, N. M. Harrison, First-principles calculations of the phase stability of TiO_2, *Phys. Rev. B* 65 (2002) 224112-1–224112-15.

[20] Z. G. Mei, Y. Wang, S. Shang, Z. K. Liu, First-principles study of the mechanical properties and phase stability of TiO_2, *Comp. Mater. Sci.* 83 (2014) 114–119.

[21] M. E. Arroyo-de Dompablo, A. Morales-Garcia, M. Taravillo, DFT+U calculations of crystal lattice, electronic structure, and phase stability under pressure of TiO_2 polymorphs, *J. Chem. Phys.* 135 (2011) 054503.

[22] P. Y. Simons, F. Dachille, The structure of TiO_2 II, a high-pressure phase of TiO_2, *Acta Cryst.* 23 (1967) 334–336.

[23] T. Arlt, M. Bermejo, M. A. Blanco, L. Gerward, J. Z. Jiang, J. Staun Olsen, J. M. Recio, High-pressure polymorphs of anatase TiO_2, *Phys. Rev. B* 61 (21) (2000) 14414–14419.

[24] S. Y. Chen, P. Shen, Laser ablation condensation of α-PbO_2-type TiO_2, *Phys. Rev. Lett.* 89 (9) (2002) 096106.

[25] K. Spektor, D. T. Tran, K. Leinenweber, U. Häussermann, Transformation of rutile to TiO_2-II in a high pressure hydrothermal environment, *J. Solid State Chem.* 206 (2013) 209–216.

[26] P. K. Linde, P. S. DeCarli, Polymorphic behavior of titania under dynamic loading, *J. Chem. Phys.* 50 (1) (1969) 319–325.

[27] Y. Cai, C. Zhang, Y. P. Feng, Dielectric properties and lattice dynamics of α-PbO_2-type TiO_2: The role of soft phonon modes in pressure-induced phase transition to baddeleyite-type TiO_2, *Phys. Rev. B* 84 (2011) 094107.

[28] J. Aarik, A. Aidla, T. Uustare, Atomic-layer growth of TiO_2-II thin films, *Philos. Mag. Lett.* 73 (3) (1996) 115–119.

[29] M. Y. Kuo, C. L. Chen, C. Y. Hua, H. C. Yang, P. Shen, Density functional theory calculations of dense TiO_2 polymorphs: implication for visible-light-responsive photocatalysts, *J. Phys. Chem. B* 109 (2005) 8693–8700.

[30] J. Pascual, J. Camassel, M. Mathieu, Fine structure in the intrinsic absorption edge of TiO_2, *Phys. Rev. B* 18 (10) (1978) 606–5614.

[31] H. Tang, K. Prasad, R. Sanjines, P. E. Schmid, F. Levy, Electrical and optical properties of TiO_2 anatase thin films, *J. Appl. Phys.* 75 (1994) 2042–2047.

[32] M. Ritala, M. Leskelä, Titanium isopropoxide as a precursor in atomic layer epitaxy of titanium dioxide thin films, *Chem. Mater.* 5 (1993) 1174–1181.

[33] K. Kukli, M. Ritala, M. Schuisky, M. Leskelä, T. Sajavaara, J. Keinonen, Atomic layer deposition of titanium oxide from TiI_4 and H_2O_2, *Chem. Vap. Deposition* 6 (6) (2000) 303–310.

[34] J. Aarik, A. Aidla, V. Sammelselg, T. Uustare, M. Ritala, M. Leskelä, Characterization of titanium dioxide atomic layer growth from titanium ethoxide and water, *Thin Solid Films* 370 (2000) 163–172.

[35] M. H. Suhail, G. Mohan Rao, S. Mohan, DC reactive magnetron sputtering of titanium structural and optical characterization of TiO_2 films, *J. Appl. Phys.* 71 (1992) 1421–1427.

[36] K. Narashimha Rao, S. Mohan, Optical properties of electron beam evaporated TiO_2 films deposited in an ionized oxygen medium, *J. Vac. Sci. Technol., A* 8 (1990) 3260–2164.

[37] M. Mosaddeq-ur-Rahman, G. Yu, T. Soga, T. Jimbo, H. Ebisu, M. Umeno, Refractive index and degree of inhomogeneity of nanocrystalline TiO_2 thin films: Effects of substrate and annealing temperature, *J. Appl. Phys.* 88 (2000) 4634–4641.

[38] L. Martinu, D. Poitras, Plasma deposition of optical films and coatings: A review, *J. Vac. Sci. Technol., A* 18 (2000) 2619–2645.

[39] D. J. Kim, S. H. Hahn, S. H. Oh, E. J. Kim, Influence of calcination temperature on structural and optical properties of TiO_2 thin films prepared by sol-gel dip coating, *Mater. Lett.* 57 (2002) 355–360.

[40] C. Yang, H. Fan, Y. Xi, J. Chen, Z. Li, Effects of depositing temperatures on structure and optical properties of TiO_2 films deposited by ion beam assisted electron beam evaporation, *Appl. Surf. Sci.* 254 (2008) 2685–2689.

[41] D. Di Claudio, A. R. Phani, S. Santucci, Enhanced optical properties of sol-gel derived TiO_2 films using microwave irradiation, *Opt. Mater.* 30 (2007) 279–284.

[42] A. Bendavid, P. J. Martin, H. Takikawa, Deposition and modification of titanium dioxide thin films by filtered arc deposition, *Thin Solid Films* 360 (2000) 241–249.

[43] R. Mechiakh, F. Meriche, R. Kremer, R. Bensaha, B. Boudine, A. Boudrioua, TiO_2 thin films prepared by sol-gel method for waveguiding applications: Correlation between the structural and optical properties, *Opt. Mater.* 30 (2007) 645–651.

[44] T. Busani, R. A. Devine, Dielectric and infrared properties of TiO_2 films containing anatase and rutile, *Semicond. Sci. Technol.* 20 (2005) 870–875.

[45] S. Sankar, K. G. Gopochandran, Effect of annealing on the structural, electrical and optical properties of nanostructured TiO_2 thin films, *Cryst. Res. Technol.* 44 (9) (2009) 989–994.

[46] K. Narasimha Rao, Influence of deposition parameters on optical properties of TiO_2 films, *Opt. Eng.* 41 (9) (2002) 2357–2364.

[47] D. J. Won, C. H. Wang, H. K. Jang, D. J. Choi, Effects of thermally induced anatase-to-rutile phase transition in MOCVD-grown TiO_2 films on structural and optical properties, *Appl. Phys. A* 73 (2001) 595–600.

[48] T. Nishide, M. Sato, H. Hara, Crystal structure and optical property of TiO_2 gels and films prepared from Ti-edta complexes as titania precursors, *J. Mater. Sci.* 35 (2000) 465–469.

[49] S. Djordjevic, K. Shang, B. Guan, S. Cheung, L. Liao, J. Basak, H.-F. Liu, S. Yoo, CMOS-compatible, athermal silicon ring modulators clad with titanium dioxide, *Opt. Express* 21 (2013) 13958–13968.

[50] Y. Jouane, Y.-C. Chang, D. Zhang, J. Luo, A.-Y. Jen, Y. Enami, Unprecedented highest electro-optic coefficient of 226 pm/V for electro-optic polymer/TiO_2 multilayer slot waveguide modulators, *Opt. Express* 22 (2014) 27725–27732.

[51] W.-K. Kuo, N.-C. Huang, H.-P. Weng, H.-H. Yu, Tunable phase detection sensitivity of transmitted-type guided-mode resonance sensor in a heterodyne interferometer, *Opt. Express* 22 (2014) 22968–22973.

[52] A. Purniawan, G. Pandraud, T. Moh, A. Marthen, K. Vakalopoulos, P. French, P. Sarro, Fabrication and optical measurements of a TiO_2-ALD evanescent waveguide sensor, *Sensor and Actuators B: Physica* 188 (2012) 127–132.

[53] K. Uchijima, T. Kita, H. Yamada, Nonlinear optical photonic crystal waveguide with TiO_2 material, *Proc. SPIE* 8626 (2013) 86261C.

[54] T. Alasaarela, L. Karvonen, H. Jussila, A. Säynätjoki, S. Mehravar, R. Norwood, N. Peyghambarian, K. Kieu, I. Tittonen, H. Lipsanen, High-quality crystallinity controlled ALD TiO2 for waveguiding applications, *Opt. Lett.* 38 (2013) 3980–3983.

[55] C. Evans, K. Shtyrkova, O. Reshef, M. Moebius, J. Bradley, S. Griesse-Nascimento, E. Ippen, E. Mazur, Multimode phase-matched third-harmonic generation in sub-micrometer-wide anatase TiO_2 waveguides, *Opt. Express* 23 (2015) 7832–7841.

[56] S. Chao, W.-H. Wang, C.-C. Lee, Low-loss dielectric mirror with ion-beam-sputtered TiO_2-SiO_2 mixed films, *Appl. Opt.* 40 (2001) 2177–2182.

[57] Y. Katano, S. Shinada, S. Nakajima, T. Kawanishi, H. Nakajima, Monolithic modelocked erbium-doped $LiNbO_3$ waveguide laser with dielectric multilayer mirror, *IEICE Electron. Express* 9 (2012) 245–249.

[58] Z. Várallyay, P. Dombi, Design of high-efficiency ultrabroadband dielectric gratings, *Appl. Opt.* 53 (2014) 5769–5774.

[59] M.-K. Wu, M. Liu, R. Bambery, M. Feng, N. Holonyak, Low power operation of a vertical cavity transistor laser via the reduction of collector offset voltage, *IEEE Photonics Technol. Lett.* 26 (2014) 1003–1006.

[60] S. Nakamura, K. Matsuda, T. Wakasugi, E. Kobayashi, G. Mizutani, S. Ushioda, T. Sekiya, S. Kurita, Optical second-harmonic generation from the anatase TiO_2(1 0 1) face, *J. Lumin*. 87–89 (2000) 862–864.

[61] A. Linsebigler, G. Lu, J. Yates, Photocatalysis on TiO_2 surfaces: principles, mechanisms, and selected results, *Chem. Rev.* 95 (1995) 735–758.

[62] J. Šubrt, J. Criado, L. Szatmáry, M. Diánez-Millán, N. Murafa, L. Péres-Maqueda, V. Brezová, Mechanochemical synthesis of visible light sensitive titanium dioxide photocatalyst, *Int. J. Photoenergy* 2011 (2011) 156941.

[63] W. Zhao, S.-C. Zhu, Y.-F. Li, Z.-P. Liu, Three-phase junction for modulating electron-hole migration in anatase–rutile photocatalysts, *Chem. Sci.* 6 (2015) 3483–3494.

[64] C. Shang, W. Zhao, Z.-P. Liu, Searching for new TiO_2 crystal phases with better photoactivity, *J. Phys. Condens. Matter.* 27 (2015) 134203.

[65] M. Cardona, G. Harbeke, Optical properties and band structure of wurtzite-type crystals and rutile, *Phys. Rev.* 137 (1965) A1467–A1476.

[66] C. Ottermann, K. Bange, Correlation between the density of TiO_2 films and their properties, *Thin Solid Films* 286 (1996) 32–34.

[67] J. Aarik, A. Aidla, A.-A. Kiisler, T. Uustare, V. Sammelselg, Effect of crystal structure on optical properties of TiO_2 films grown by atomic layer deposition, *Thin Solid Films* 305 (1997) 270–273.

[68] A. Bendavid, P. Martin, Å. Jamting, H. Takikawa, Structural and optical propertiesof titanium dioxide thin films deposited by filtered arc deposition, *Thin Solid Films* 355–356 (1999) 6–11.

[69] D. Mergel, Modeling thin TiO_2 films of various densities as an effective optical medium, *Thin Solid Films* 397 (2001) 216–222.

[70] T. Sumita, T. Yamaki, S. Yamamoto, A. Miyashita, Photoinduced charge separation of highly oriented TiO_2 anatase and rutile thin films, *Appl. Surf. Sci.* 200 (2002) 21–26.

[71] L. Miao, P. Jin, K. Kaneko, A. Terai, N. Nabatova-Gabain, S. Tanemura, Preparation and characterization of polycrystalline anatase and rutile TiO_2 thin films by rf magnetron sputtering, *Appl. Surf. Sci.* 212–213 (2003) 255–263.

[72] J. Aarik, A. Aidla, H. Mändar, T. Uustare, M. Schuisky, A. Hårsta, Atomic layer growth of epitaxial TiO_2 films from $TiCl_4$ and H_2O on α-Al_2O_3 substrates, *J. Cryst. Growth* 242 (2002) 189–198.

[73] L. Aarik, T. Arroval, R. Rammula, H. Mändar, V. Sammelselg, J. Aarik, Atomic layer deposition of TiO_2 from $TiCl_4$ and O_3, *Thin Solid Films* 542 (2013) 100–107.

[74] H. Murata, Y. Kataoka, T. Kawamoto, I. Tanaka, T. Taniguchi, Photocatalytic activity of α-PbO_2-type TiO_2, *Phys. Status Solidi RRL* 10 (2014) 822–826.

[75] H. Razavi-Khosroshahi, K. Edalati, M. Hirayama, H. Emami, M. Arita, M. Yamauchi, H. Hagiwara, S. Ida, T. Ishihara, E. Akiba, Visible-light-driven photocatalytic hydrogen generation on nanosized TiO_2-II stabilized by high-pressure torsion, *ACS Catal.* 6 (2016) 5103–5107.

[76] K. Edalati, Q. Wang, H. Eguchi, H. Razavi-Khosroshahi, H. Emami, M. Yamauchi, M. Fuji, Z. Horita, Impact of TiO_2-II phase stabilized in anatase matrix by high-pressure torsion on electrocatalytic hydrogen production, *Mater. Res. Lett.* 7 (2019) 334–339.

[77] K. Mukai, I. Yamada, Columbite-type TiO_2 as a negative electrode material for lithium-ion batteries, *J. Electrochem. Soc.* 164 (2017) A3590–A3594.

[78] Y. Tang, Y. Li, W. Guo, J. Wang, X. Li, S. Chen, S. Mu, Y. Zhao, F. Gao, A highly ordered multi-layered hydrogenated TiO_2-II phase nanowire array negative electrode for 2.4 eV aqueous asymmetric supercapacitors with high energy density and long cycle life, *J. Mater. Chem.* 6 (2018) 623–632.

[79] D. W. Meng, X. L. Wu, F. Sun, L. W. Huang, F. Liu, Y. J. Han, J. P. Zheng, X. Meng, R. Mason, High-pressure polymorphic transformation of rutile to α-PbO_2-type TiO_2 at {011}R twin boundaries, *Micron* 39 (2008) 280–286.

[80] H. Chang, H. You, J. Guo, D. Lam, Epitaxial TiO_2 and VO_2 films prepared by MOCVD, *Appl. Surf. Sci* 48–49 (1991) 12–18.

[81] K. Fröhlich, M. Ťapajna, A. Rosová, E. Dobročka, K. Hušeková, J. Aarik, A. Aidla, Growth of high-dielectric-constant TiO_2 films in capacitors with RuO_2 electrodes, *Electrochem. Solid State Lett.* 11 (2008) G19–G21.

[82] X. Jiang, H. Huang, F. B. Prinz, S. F. Bent, Application of Atomic Layer Deposition of Platinum to Solid Oxide Fuel Cells, *Chem. Mater.* 20 (12) (2008) 3897–3905.

[83] R. Warren, F. Sammoura, F. Tounsi, M. Sanghadasac, L. Lin, Highly active ruthenium oxide coating via ALD and electrochemical activation in supercapacitor applications, *J. Mater. Chem. A* 3 (2015) 15568–15575.

[84] B. J. O'Neill, D. H. K. Jackson, J. Lee, C. Canlas, P. C. Stair, C. L. Marshall, J. W. Elam, T. F. Kuech, J. A. Dumesic, G. W. Huber, Catalyst Design with Atomic Layer Deposition, *ACS Catal.* 5 (3) (2015) 1804–1825.

[85] T. Suntola, Atomic layer epitaxy, *In: Handbook of Crystal Growth, Elsevier Science* (1994) 601–663.

[86] M. Ritala, M. Lesklä , E. Nykänen, P. Soininen, L. Niinistö, Growth of titanium dioxide thin films by atomic layer epitaxy, *Thin Solid Films* 255 (1993) 288–295.

[87] J. Aarik, A. Aidla, T. Uustare, V. Sammelselg, Morphology and structure of TiO_2 thin films grown by atomic layer deposition, *J. Cryst. Growth* 148 (1995) 268–275.

[88] J. Aarik, A. Aidla, H. Mändar, V. Sammelselg, Anomalous effect of temperature on atomic layer deposition of titanium dioxide, *J. Cryst. Growth* 220 (2000) 531–537.

[89] J. Aarik, A. Aidla, T. Uustare, M. Ritala, M. Leskelä, Titanium isopropoxide as a precursor for atomic layer deposition: characterization of titanium dioxide growth process, *Appl. Surf. Sci.* 161 (2000) 385–395.

[90] J. Aarik, A. Aidla, H. Mändar, T. Uustare, Atomic layer deposition of titanium dioxide from $TiCl_4$ and H_2O: investigation of growth mechanism, *Appl. Surf. Sci.* 172 (2001) 148–158.

[91] M. Schuisky, K. Kukli, J. Aarik, J. Lu, A. Hårsta, Epitaxial growth of TiO_2 films in a hydroxyl-free atomic layer deposition process, *J. Cryst. Growth* 235 (2002) 293–299.

[92] V. F. Silva, V. Bouquet, S. Deputier, S. Boursicot, S. Ollivier, I. T. Weber, V. L. Silva, I. M. G. Santos, M. Guilloux-Viry, A. Perrin, Substrate-controlled allotropic phases and growth orientation of TiO_2 epitaxial thin films, *J. Appl. Crystallogr.* 43 (6) (2010) 1502–1512.

[93] R. L. Puurunen, T. Sajavaara, E. Santala, V. Miikkulainen, T. Saukkonen, M. Laitinen, M. Leskelä, Controlling the crystallinity and roughness of atomic layer deposited titanium dioxide films, *J. Nanosci. Nanotechnol.* 11 (2011) 8101–8107.

[94] L. B. Freud, S. Suresh, Thin Film Materials, *Cambridge University Press*, 2006.

[95] A. S. Cooper, Precise lattice constants of germanium, aluminum, gallium, arsenide, uranium, sulphur, quartz and sapphire, *Acta Cryst.* 15 (1962) 578–582.

[96] M. Lucht, M. Lerche, H. C. Wille, Y. V. Shvyd'ko, H. D. Rüter, E. Gerdau, P. Becker, Precise measurement of the lattice parameters of sapphire in the temperature range 4.5 K–250 K using the Mössbauer wavelenght standard, *J. Appl. Cryst.* 36 (4) (2003) 1075–1081.

[97] H. V. Hart, H. G. Drickamer, Effect of high pressure on the lattice parameters of Al_2O_3, *J. Chem. Phys.* 43 (1965) 2265–2267.

[98] S. Halfner, M. Raymond, Selfconsistent ionic potentials, fields, and field gradients at the lattice sites of corundum (Al_2O_3), *J. Chem. Phys.* 49 (1968) 3570–3579.

[99] J. Narayan, K. Dovidenko, A. K. Sharma, S. Oktyabrsky, Defects and interfaces in epitaxial ZnO/Al_2O_3 and $AIN/ZnO/Al_2O_3$ heterostructures, *J. Appl. Phys.* 84 (1998) 2597–2601.

[100] J. Aarik, J. Karlis, H. Mändar, T. Uustare, V. Sammelselg, Influence of structure development on atomic layer deposition of TiO_2 thin films, *Appl. Surf. Sci.* 181 (2001) 339–348.

[101] L. Avril, S. Reymond-Laruinaz, J. M. Decams, S. Bruyere, V. Potin, M. C. Marco de Lucas, L. Imhoff, TiO_2 anatse films obtained by direct liquid injection atomic layer deposition at low temperature, *Appl. Surf. Sci.* 288 (2014) 201–207.

[102] V. Pore, A. Rahtu, M. Leskelä, M. Ritala, T. Sajavaara, J. Keinonen, Atomic layer deposition of photocatalytic TiO_2 thin films from titanium tetramethoxide and water, *Chem. Vap. Deposition* 10 (3) (2004) 143–148.

[103] M. Schuisky, A. Harsta, A. Aidla, K. Kukli, A.-A. Kiisler, J. Aarik, Atomic layer chemical vapor deposition of TiO_2 low temperature epitaxy of rutile and anatase, *J. Electrochem. Soc.* 147 (9) (2000) 3319–3325.

[104] J. Aarik, A. Aidla, T. Uustare, K. Kukli, V. Sammelselg, M. Ritala, M. Leskelä, Atomic layer deposition of TiO_2 thin films from TiI_4 and H_2O, *Appl. Surf. Sci.* 193 (2002) 277–286.

[105] J. Hidalgo-Jimenes, Q. Wang, K. Edalati, J. Cubero-Sesín, H. Razavi-Khosroshahi, Y. Ikoma, D. Gutiérrez-Fallas, F. Dittel-Meza, J. Rodríguez-Rufino, M. Fuji, Phase transformations, vacancy formation and variations of optical and photocatalytic properties in TiO_2-ZnO composites by high-pressure torsion, *Int. J. Plast.* 124 (2020) 170–185.

[106] Y. Wang, K. Saitow, Mechanochemical synthesis of red-light-active green TiO_2 photocatalysts with disorder: Defect-rich, with polymorphs, and no metal loading, *Chem. Mater.* 32 (2020) 9190–9200.

[107] A. Das, B. Chowdhury, R. Saha, S. Sikdar, S. Bhunia, S. Chattopadyay, Ultrathin vapor-liquid-solid grown titanium dioxide-II film on bulk GaAs substrates for advanced metal-oxide-semiconductor device applications, *IEEE Trans. Electron Devices* 65 (2018) 1466–1472.

[108] M. Pushpa, M. Crespo, M. Cristopher, P. Karthick, M. Sridharam, C. Sanjeeviraja, K. Jeyadheepan, Influence of pyrolytic temperature on optoelectronic properties and the energy harvesting applications of high pressure TiO_2 thin films, *Vacuum* 161 (2019) 81–91.

[109] N. Bendeliany, S. Popova, O. Vereshchagin, New modification of titanium dioxide obtained at high pressures, *Geochemistry* 5 (1966) 499–501.

[110] R. McQueen, J. Jamieson, S. Marsh, Shock-wave compression and X-ray studies of titanium dioxide, *Science* 155 (1967) 1401–1404.

[111] T. Sekiya, S. Ohta, S. Kamei, M. Hanakawa, S. Kurita, Raman spectroscopy and phase transition of anatase TiO_2 under high pressure, *J. Phys. Chem. Solids* 62 (2001) 717–721.

[112] S. Ohta, T. Sekiya, S. Kurita, Pressure dependence of optical properties of anatase TiO_2 single crystal, *Phys. Stat. Sol. B* 223 (2001) 265–269.

[113] W. Liu, J. Chen, X. Zhang, J. Yan, M. Hou, M. Kunz, D. Zhang, H. Zhang, Pressure-induced phase transitions of natural brookite, *ACS Earth Space Chem.* 3 (2019) 844–853.

[114] S. Begin-Colin, G. Le Caer, A. Mocellin, M. Zadona, Polymorphic transformations of titania induced by ball milling, *Philos. Mag. Lett.* 69 (1994) 1–7.

[115] M. Rinaudo, A. Beltrán, M. Fernández, L. Cadús, M. Morales, Tailoring materials by high-energy ball milling: TiO_2 mixtures for catalyst support applications, *Mater. Today Chem.* 17 (2020) 100340.

[116] Q. Wang, M. Watanabe, K. Edalati, Visible-light photocurrent in nanostructured high-pressure TiO_2-II (columbite) phase, *J. Phys. Chem.* 124 (2020) 13930–13935.

[117] S. Filatov, N. Bendeliani, B. Albert, J. Kopf, T. Dyuzheva, L. Lityagina, Crystalline Structure of the TiO_2 II High-Pressure Phase at 293, 223, and 133 K According to Single-Crystal X-ray Diffraction Data, *Dokl. Phys.* 52 (2007) 195–199.

[118] D. Mitchell, G. Triani, D. Attard, K. Finnie, P. Evans, C. Barbé, J. Bartlett, Atomic layer deposition of TiO_2 and Al_2O_3 thin films and nanolaminates, *Smart Mater. Struct.* 15 (2006) S57–S64.

[119] A. Kasikov, J. Aarik, H. Mändar, M. Moppel, M. Pärs, T. Uustare, Refractive index gradients in TiO_2 thin films grown by atomic layer deposition, *J. Phys. D: Appl. Phys.* 39 (2006) 54–60.

[120] S. Xiao, U. Dahmen, A. Heuer, Phase trasformation of TiO_2 precipitates in sapphire (α-Al_2O_3) induced by the loss of coherency, *Philos. Mag. A* 71 (1) (1997) 221–238.

[121] J. Aarik, A. Aidla, A. Jaek, M. Leskelä, L. Niinistö, In situ study of a strontium β-diketonate precursor for thin film growth by atomic layer epitaxy, *J. Mater. Chem.* 4 (1994) 1239–1244.

[122] T. Arroval, L. Aarik, R. Rammula, V. Kruusla, J. Aarik, Effect of substrate-enhanced and inhibited growth on atomic layer deposition and properties of aluminum-titanium oxide films, *Thin Solid Films* 600 (2016) 119–125.

[123] H. Mändar, J. Felsche, V. Mikli, T. Vajakas, AXES1.9: new tools for estimation of crystallite size and shape by Williamson–Hall analysis, *J. Appl. Crystallogr.* 32 (2) (1999) 345–350.

[124] F. Campanale, E. Mugnaioli, L. Folco, P. Parlanti, M. Gemmi, TiO_2 II: The high-pressure Zr-free srilankite endmember in impact rocks, *Meteoritics & Planetary Science* 59 (2024) 529–543.

[125] R. Swanepoel, Determination of the thickness and optical constants of amorphous silicon, *J. Phys. E: Sci. Instrum.* 16 (1983) 1214–1222.

[126] J. Rodríguez, M. Gómez, J. Ederth, G. Niklasson, C. Granqvist, Thickness dependence of the optical properties of sputter deposited Ti oxide films, *Thin Solid Films* 365 (2000) 119–125.

[127] N. Hosaka, T. Sekiya, C. Satoko, S. Kurita, Optical properties of single-crystal anatase TiO_2, *Phys. Soc. Japan* 66 (1997) 877–880.

[128] J. Rams, A. Tejeda, J. M. Cabrera, Refractive indices of rutile as a function of temperature and wavelength, *J. Appl. Phys.* 82 (1997) 994–997.

[129] G. E. Jellison, L. A. Boatner, J. D. Budai, B.-S. Jeong, D. P. Norton, Spectroscopic ellipsometry of thin film and bulk anatase (TiO_2), *J. Appl. Phys.* 93 (2003) 9537–9541

[130] A. Gordeeva, T. Thersleff, Y.-J. Hsu, C. Liebske, P. Ulmer, O. Andersson, U. Häussermann, Electronic structure characterization of TiO_2-II with the α-PbO_2 structure by electron-energy-loss-spectroscopy and comparison with anatase, brookite, and rutile, *J. Solid State Chem.* 322 (2023) 123952.

[131] V. Kulikovsky, R. Ctvrtlik, V. Vorlicek, J. Filip, P. Bohac, L. Jastrabik, Mechanical properties and structure of TiO_2 films deposited on quartz and silicon substrates, *Thin Solid Films* 542 (2013) 91–99.

[132] O. Ylivaara, A. Langner, X. Liu, D. Schneider, J. Julin, K. Arstila, S. Sintonen, S. Ali, H. Lipsanen, T. Sajavaara, Mechanical and optical properties of as-grown and thermally annealed titanium dioxide from titanium tetrachloride and water by atomic layer deposition, *Thin Solid Films* 732 (2021) 138758.

PUBLICATIONS

CURRICULUM VITAE

Name: Kristel Möls (Möldre)
Date of Birth: 04.01.1989
E-mail: kristel.mols@ut.ee, kristel.moldre@gmail.com

Education:

2014–	Tartu Ülikool, doctorate studies, material science
2012–2014	Tartu Ülikool, master's studies, material science
2009–2012	Tartu Ülikool, bachrlor's studies, material science

Work experience

01.11.2022–	Karl Storz Video Endoscopy Estonia OÜ, LEAN engineer
01.10.2021–31.10.2022	AS Norma, serial production process engineer
01.07.2016–31.01.2021	University of Tartu, Faculty of Science and Technology, Institute of Physics, Engineer (0.80)
01.04.2015–31.08.2016	Health Board, senior specialist
01.05.2014–30.06.2015	University of Tartu, Faculty of Science and Technology, Institute of Physics, engineer (0.40)
04.07.2011–30.06.2012	University of Tartu, Faculty of Science and Technology, Institute of Physics, laboratory assistant (0.25)

Publications:

A. Tarre, **K. Möldre**, A. Niilisk, H. Mändar, J. Aarik, A. Rosental, Atomic layer deposition of epitaxial TiO_2-II on c-sapphire, *Journal of Vacuum Science & Technology A: Vacuum Surfaces and Films* 31 (1) (2013) 01A118-1–5, http://doi.org/10.1116/1.4764892.

K. Möldre, L. Aarik, H. Mändar, A. Niilisk, R. Rammula, A. Tarre, J. Aarik, Atomic layer deposition of rutile and TiO_2-II from $TiCl_4$ and O_3 on sapphire: Influence of substrate orientation on thin film structure, *Journal of Crystal Growth* 428 (2015) 86–92, https://doi.org/10.1016/j.jcrysgro.2015.07.029.

K. Möls, L. Aarik, H. Mändar, A. Kasikov, A. Niilisk, R. Rammula, J. Aarik, Influence of phase composition on optical properties of TiO_2: Dependence of refractive index and band gap on formation of TiO_2-II phase in thin films, *Optical Materials* 96 (2019) 109335, https://doi.org/10.1016/j.optmat.2019.109335.

K. Möls, L. Aarik, H. Mändar, A. Kasikov, T. Jõgiaas, A. Tarre, J. Aarik, Influence of α-Al_2O_3 template and process parameters on atomic layer deposition and properties of thin films containing high-density TiO_2 phases, *Coatings* 11 (11) (2021) 1280, https://doi.org/10.3390/coatings11111280.

Conference presentations:

K. Möls, H. Mändar, T. Jõgiaas, J. Aarik, Influence of TiO_2-II on hardness of titanium dioxide thin films, GSFMT Scientific Conference 2023, Tartu, May 23–24, 2023.

K. Möls, L. Aarik, A. Tarre, H. Mändar, A. Kasikov, A. Niilisk, J. Aarik, Synthesis and properties of titania films containing anatase, rutile and high-pressure TiO_2-II, GSFMT Scientific Conference 2021, Tartu, June 14–15, 2021.

K. Möldre, L. Aarik, H. Mändar, J. Aarik, Atomic layer deposition of TiO_2 on α-Al_2O_3(001): influence of substrate temperature on epitaxial growth and phase composition of thin films, 16th International Conference on Atomic Layer Deposition, Dublin, July 24–27, 2016.

K. Mõldre, L. Aarik, A. Tarre, H. Mändar, L. Puust, V. Kiisk, I. Sildos, J. Aarik, Optical properties of TiO_2-II grown by atomic layer deposition, 13th International Baltic Conference on Atomic Layer Deposition, Tartu, September 27–29, 2015.

K. Möldre, H. Mändar, L. Aarik, A. Tarre, J. Aarik, Structure characterization of lattice-matched rutile and TiO_2-II phases grown by atomic layer deposition on α-Al_2O_3(001), 29th European Crystallographic Meeting, Rovinj, August 23–28, 2015.

K. Möldre, L. Aarik, A. Tarre, H. Mändar, J. Aarik, Atomic layer deposition of TiO_2 on sapphire: Effect of substrate orientation on structure and growth rate of thin films, 12th International Baltic Conference on Atomic Layer Depostion, Helsinki, Finland Helsinki, May 12–13, 2014.

K. Möldre, A. Tarre, P. Adamson, T. Kahro, A. Niilisk, J. Aarik, Real-time optical characterization of atomic layer deposition of dielectrics on graphene, International Conference Functional Materials and Nanotechnologies 2013 – FM&NT2013, Tartu, April 21–24, 2013.

ELULOOKIRJELDUS

Nimi:	Kristel Möls (Möldre)
Sünniaeg:	04.01.1989
E-mail:	kristel.mols@ut.ee, kristel.moldre@gmail.com

Hariduskäik:

2014–	Tartu Ülikool, doktoriõpe, materjaliteadus
2012–2014	Tartu Ülikool, magistriõpe, materjaliteadus
2009–2012	Tartu Ülikool, bakalaureuseõpe, materjaliteadus

Töökohad ja ametid

01.11.2022–	Karl Storz Video Endoscopy Estonia OÜ, LEAN insener
01.10.2021–31.10.2022	AS Norma, seeriatootmise protsessiinsener
01.07.2016–31.01.2021	Tartu Ülikool, Loodus- ja täppisteaduste valdkond, füüsika instituut, insener (0.80)
01.04.2015–31.08.2016	Terviseamet, vanemspetsialist
01.05.2014–30.06.2015	Tartu Ülikool, Loodus- ja tehnoloogiateaduskond, füüsika instituut, insener (0.40)
04.07.2011–30.06.2012	Tartu Ülikool, Loodus- ja tehnoloogiateaduskond, füüsika instituut, laborant (0.25)

Publikatsioonid:

A. Tarre, **K. Möldre**, A. Niilisk, H. Mändar, J. Aarik, A. Rosental, Atomic layer deposition of epitaxial TiO_2 II on c-sapphire, *Journal of Vacuum Science & Technology A: Vacuum Surfaces and Films* 31 (1) (2013) 01A118-1–5, http://doi.org/10.1116/1.4764892.

K. Möldre, L. Aarik, H. Mändar, A. Niilisk, R. Rammula, A. Tarre, J. Aarik, Atomic layer deposition of rutile and TiO_2-II from $TiCl_4$ and O_3 on sapphire: Influence of substrate orientation on thin film structure, *Journal of Crystal Growth* 428 (2015) 86–92, https://doi.org/10.1016/j.jcrysgro.2015.07.029.

K. Möls, L. Aarik, H. Mändar, A. Kasikov, A. Niilisk, R. Rammula, J. Aarik, Influence of phase composition on optical properties of TiO_2: Dependence of refractive index and band gap on formation of TiO_2-II phase in thin films, *Optical Materials* 96 (2019) 109335, https://doi.org/10.1016/j.optmat.2019.109335.

K. Möls, L. Aarik, H. Mändar, A. Kasikov, T. Jõgiaas, A. Tarre, J. Aarik, Influence of α-Al_2O_3 template and process parameters on atomic layer deposition and properties of thin films containing high-density TiO_2 phases, *Coatings* 11 (11) (2021) 1280, https://doi.org/10.3390/coatings11111280.

Konverentsiettekanded:

K. Möls, H. Mändar, T. Jõgiaas, J. Aarik, Influence of TiO_2-II on hardness of titanium dioxide thin films, GSFMT Scientific Conference 2023, Tartu, May 23.–24, 2023.

K. Möls, L. Aarik, A. Tarre, H. Mändar, A. Kasikov, A. Niilisk, J. Aarik, Synthesis and properties of titania films containing anatase, rutile and high-pressure TiO_2-II, GSFMT Scientific Conference 2021, Tartu, June 14.–15, 2021.

K. Möldre, L. Aarik, H. Mändar, J. Aarik, Atomic layer deposition of TiO_2 on α-Al_2O_3(001): influence of substrate temperature on epitaxial growth and phase composition of thin films, 16th International Conference on Atomic Layer Deposition, Dublin, July 24–27, 2016.

K. Mõldre, L. Aarik, A. Tarre, H. Mändar, L. Puust, V. Kiisk, I. Sildos, J. Aarik, Optical properties of TiO_2-II grown by atomic layer deposition, 13th International Baltic Conference on Atomic Layer Deposition, Tartu, September 27–29, 2015.

K. Möldre, H. Mändar, L. Aarik, A. Tarre, J. Aarik, Structure characterization of lattice-matched rutile and TiO_2-II phases grown by atomic layer deposition on α-Al_2O_3(001), 29th European Crystallographic Meeting, Rovinj, August 23–28, 2015.

K. Möldre, L. Aarik, A. Tarre, H. Mändar, J. Aarik, Atomic layer deposition of TiO_2 on sapphire: Effect of substrate orientation on structure and growth rate of thin films, 12th International Baltic Conference on Atomic Layer Depostion, Helsinki, Finland Helsinki, May 12–13, 2014.

K. Möldre, A. Tarre, P. Adamson, T. Kahro, A. Niilisk, J. Aarik, Real-time optical characterization of atomic layer deposition of dielectrics on graphene, International Conference Functional Materials and Nanotechnologies 2013 – FM&NT2013, Tartu, April 21–24, 2013.

DISSERTATIONES SCIENTIAE MATERIALIS UNIVERSITATIS TARTUENSIS

1. **Martin Järvekülg**. Tubular microstructures by Hf-, Zr- and Ti-butoxide gel sheet rolling. Tartu, 2011, 112 p.
2. **Sergei Vlassov.** Investigation of nanoscale interactions and mechanical properties of nanostructures using quartz tuning fork based real-time measurements. Tartu, 2011, 171 p.
3. **Margus Kodu**. Pulsed Laser Deposition of Magnesium Oxide and Barium Ternary Oxides for Plasma Display Protective Layers. Tartu, 2011, 89 p.
4. **Rainer Pärna**. Surface studies of some oxide films. Tartu, 2011, 129 p.
5. **Jevgeni Šulga**. Self-assembly and interaction of nanostructures. Tartu, 2011, 114 p.
6. **Wojciech Kuznik**. Quantum-chemical computer simulations of the linear and non-linear optical properties of pyrazoloquinoline and dicyanopyrazine derivatives. Tartu, 2012, 89 p.
7. **Leonid Dorogin**. Structural and tribological properties of zero- and one-dimensional nanocrystals. Tartu, 2012, 193 p.
8. **Viljar Palmre**. Fabrication and characterization of microporous carbon-based electroactive polymer actuators. Tartu, 2012, 99 p.
9. **Madis Paalo**. Synthesis of CNT-metal oxide nanocomposites: sol-gel process, rheology, structural and functional properties. Tartu, 2014, 175 p.
10. **Raul Välbe**. Developement of ionic liquid composites by sol-gel method for elaboration of industrial nano- and microstructures. Tartu, 2014, 97 p.
11. **Urmas Joost**. Impurity and preparation dependent properties of titania thin films. Tartu, 2014, 155 p.
12. **Madis Umalas**. Application of sol-gel technology for production of ceramic nanocomposites and functional coatings. Tartu, 2015, 136 p.
13. **Elena Samsonova**. Energy transfer probe as a tool to study morphological and structural origins of fluorescence quenching in rare-earth doped nanophosphors. Tartu, 2015, 114 p.
14. **Jay Mondal**. Novel Corrosion Protective Nanostructured Composite Coatings. Tartu, 2016, 104 p.
15. **Kathriin Utt**. Metal oxide mesostructures for optical applications. Tartu, 2016, 88 p.
16. **Kaido Siimon**. Electrospun gelatin cross-linked by glucose. Tartu, 2016, 84 p.
17. **Marko Part**. Combined three-dimensional sol-gel structures and atomic layer deposited thin films. Tartu, 2017, 162 p.
18. **Pejman Rasti**. Analysis of Remote Sensing Image Super Resolution using Fluid Lenses. Tartu, 2017, 188 p.
19. **Ivo Romet**. Recombination luminescence of doped borates: origin and application prospects in dosimetry. Tartu, 2017, 111 p.

20. **Vladimir I. Kondratiev**. Processing and characterization of transparent electrode materials. Tartu, 2017, 111 p.
21. **Taivo Jõgiaas**. Mechanical properties of atomic layer deposited thin films and nanocomposites. Tartu, 2017, 125 p.
22. **Lauri Aarik**. Atomic layer deposition and characterization of thin oxide films for application in protective coatings. Tartu, 2017, 180 p.
23. **Triin Kangur**. Preparation and functional properties of stochastic microstructured sol-gel silica materials. Tartu, 2018, 96 p.
24. **Marta Berholts**. Fragmentation of ionic and hydrogen-bonded molecules induced by synchrotron radiation. Tartu, 2018, 126 p.
25. **Priit Priimägi**. Development and optimization of 3D-microbatteries. Tartu, 2018, 118 p.
26. **Siim Hödemann**. Residual stress determination in chemically strengthened and thermally tempered glass plates using scattered light method. Tartu, 2019, 146 p.
27. **Jekaterina Kozlova**. Complex characterization of graphene structures on nanometer level. Tartu, 2019, 206 p.
28. **Kristjan Kalam**. Magnetic, electric and structural properties of atomic layer deposited zirconia-based nanolaminates and mixtures. Tartu, 2020, 94 p.
29. **Triinu Vihmann**. Ionic liquids: synthesis and application in lubrication and lithography. Tartu, 2020, 102 p.
30. **Helina Seemen**. Atomic layer deposition and microscopic analysis of magnetically and electrically polarizable thin solid films. Tartu, 2021, 126 p.
31. **Ekaterina Vagapova**. Fluorescence quenching in inorganic crystalline solids activated by neodymium ions; from bulk to micro- and nanocrystals. Tartu, 2021, 116 p.
32. **Evgenii Strugovshchikov**. First-principles studies on rare-earth metal-hydride-based smart materials. Tartu, 2021, 166 p.
33. **Maido Merisalu**. Nanostructured Coatings for Car and Aerospace Industries. Tartu, 2022, 179 p.
34. **Elena Vinogradova**. Optical centers and quantum entangled states of Nd3+ ions in doped fluoride crystals. Tartu, 2023, 92 p.
35. **Dmytro Danilian**. “Photocatalytic materials for water treatment and antimicrobial applications”. Tartu, 2024, 139 p.